Single crystal growth of water-soluble metal complexes with the help of the nano-crystallization method

Alvarez, Ricardo ; Nievergelt, Philipp P ; Slyshkina, Ekaterina ; Müller, Peter ; Alberto, Roger ; Spingler, Bernhard

Abstract: The Nano-Crystallization method has been extensively tested for the growth of single crystals of cationic coordination compounds, which are soluble in water. All three studied, diverse metal complexes could be crystallized with the help of pipetting robots commonly used for the crystallization of proteins and the anion small molecule screen. It was furthermore possible to obtain for each positively charged complex several structures with different anions. In one case, together with literature data, a total of six salts with different anions could be assembled, which allowed an investigation of the influence of the counterions on the inter-cation metal-to-metal distance. The Nano-Crystallization method can be recommended for the single crystal growth of cationic coordination complexes, which are stable in water and have an aqueous solubility of at least 2 mM. This is the first publication dedicated solely to the single crystal growth of coordination complexes.

DOI: https://doi.org/10.1039/d0dt01236j

Originally published at:
Alvarez, Ricardo; Nievergelt, Philipp P; Slyshkina, Ekaterina; Müller, Peter; Alberto, Roger; Spingler, Bernhard (2020). Single crystal growth of water-soluble metal complexes with the help of the nano-crystallization method. Dalton Transactions, 49(28):9632-9640.
DOI: https://doi.org/10.1039/d0dt01236j

Dalton Transactions

ROYAL SOCIETY OF CHEMISTRY

PAPER

Cite this: *Dalton Trans.*, 2020, **49**, 9632

Single crystal growth of water-soluble metal complexes with the help of the nano-crystallization method†

Ricardo Alvarez, Philipp P. Nievergelt, Ekaterina Slyshkina, Peter Müller, Roger Alberto and Bernhard Spingler *

Received 2nd April 2020,
Accepted 23rd June 2020

DOI: 10.1039/d0dt01236j

rsc.li/dalton

The Nano-Crystallization method has been extensively tested for the growth of single crystals of cationic coordination compounds, which are soluble in water. All three studied, diverse metal complexes could be crystallized with the help of pipetting robots commonly used for the crystallization of proteins and the anion small molecule screen. It was furthermore possible to obtain for each positively charged complex several structures with different anions. In one case, together with literature data, a total of six salts with different anions could be assembled, which allowed an investigation of the influence of the counterions on the inter-cation metal-to-metal distance. The Nano-Crystallization method can be recommended for the single crystal growth of cationic coordination complexes, which are stable in water and have an aqueous solubility of at least 2 mM. This is the first publication dedicated solely to the single crystal growth of coordination complexes.

1. Introduction

In most cases, setting up the crystallization of a small molecule is a manual process. If done intentionally, a solution of the compound is prepared and then the conditions are changed in order to reach supersaturation, which is hopefully followed by crystallization.[1] While there are dedicated publications that deal exclusively with the crystallization of organic compounds,[2] there are no publications to the best of our knowledge that are solely dedicated to the growth of single crystals of coordination metal complexes (see however the following references for the (single) crystal growth of MOFs from aqueous solutions,[3] for the high-throughput synthesis of crystalline MOF materials[4] and for the measurement of microcrystals of reactive coordination complexes[5]). This is really surprising, as 57% of the entries in the Cambridge Structure Database[6] contain a metal ion. We have recently developed a crystallization screen consisting of 77 different anions and have successfully applied the screen for the crystallization of six out of seven very diverse organic cations, which were all water soluble to at least a concentration of 2 mM.[7] The 96 different solutions of the screen are either mixed with the help of a pipetting robot[7a] or just with a cheap multi-channel pipette under oil.[7b] Vapor diffusion of water from the crystallization drops either in the bigger reservoir[7a] or through the oil into the air,[7b] induces the growth of the crystals. The first coordination complex crystallized by this technique has just been reported.[8]

With coordination metal complex cations, the counteranion has an influence upon various structural aspects such as dimensionality, topology and nuclearity, and other parameters dependent on the structure, such as the magnetic behavior of cobalt(II),[9] copper(II),[10] zinc(II),[11] silver(I),[12] cadmium(II),[13] mercury(II)[14] and dysprosium(III)[15] coordination complexes. It is a common feature of these studies that they are limited to simple anions, whose metal salts are already commercially available and which serve as starting materials for the complex formation. Bugris *et al.* described the calcium(II) complexes of two similar polyhydroxy carboxylates, gluconate and isosaccharinate.[16] These two structures display very different shortest metal to metal distances of 3.7312(2) Å and 5.734(1) Å respectively, because in the first case a μ-oxo bridge formed by the carboxylate was present but not in the latter.

In the course of this study, we wanted to evaluate systematically the crystallization behavior of selected cationic coordination complexes using our newly developed Nano-Crystallization technique.[7a] For this purpose, we chose the racemic chloride salts of cobalt(III) tris(bipyridine) (**1**)[17] and

Department of Chemistry, University of Zurich, 8057 Zurich, Switzerland.
E-mail: spingler@chem.uzh.ch

†Electronic supplementary information (ESI) available: Detailed description and crystallographic data for **1a–1c**, **2a**, **2b**, **4a–4d**, in CIF format, additional structural figures and experimental characterizations. CCDC 1986517–1986525. For ESI and crystallographic data in CIF or other electronic format see DOI: 10.1039/d0dt01236j

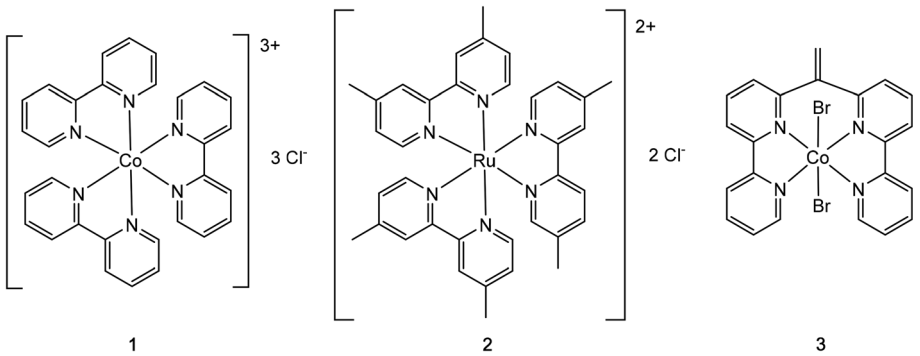

Fig. 1 The tested coordination complexes for single crystal growth by the anion exchange Nano-Crystallization method: [Co(III)(2,2′-bipyridine)$_3$](chloride)$_3$ (**1**), [Ru(II)(4,4′-dimethyl-2,2′-bipyridine)$_3$](chloride)$_2$ (**2**), and Co(II)(6,6′′-(ethene-1,1-diyl)di-2,2′-bipyridine)(bromide)$_2$ (**3**).

ruthenium(II) tris(4,4′-dimethyl-2,2′-bipyridine) (**2**)[18] as well as cobalt(II)(6,6″-(ethene-1,1-diyl)di-2,2′-bipyridine)(bromide)$_2$ (**3**) as test candidates (Fig. 1). While complex **3** was expected to allow direct coordination of some exchanged anions to the metal center, this direct coordination mode was assumed to be unlikely in the case of the coordinatively saturated metal centers in **1** and **2**. Cobalt(III) tris(bipyridine) and ruthenium(II) tris(bipyridine) complexes are important in many light-to-energy applications like dye-sensitized solar cells (DSSC).[19] DSSCs use a wide band-gap semiconductor, which is sensitized to visible light by an adsorbed dye molecule and an electrolyte containing a redox mediator.[20] Cobalt(III) tris(2,2′-bipyridine) complexes are used as high-performing dye-regenerating mediators in DSSC. Compared to iodide, the traditional mediator used in DSSC, cobalt complexes are noncorrosive to the metal cathodes and tend to compete less with the dye for visible light and most importantly have synthetically tunable redox potentials.[19a] Ruthenium(II) polypyridine complexes and their derivatives have been tested extensively as photosensitizers in DSSC.[20a,21] Another area of use for ruthenium(II) tris-bipyridine complexes is the excited-state proton-coupled electron transfer (PCET), in which two ruthenium(II) tris-bipyridine cations are connected by a salt bridge to facilitate the proton transfer.[19b] So far, only two crystal structures have been reported that contain the cobalt(III) tris(2,2′-bipyridine) cation with a simple anion.[22] Analogously, only two reported crystal structures describe the cationic ruthenium(II) tris(4,4′-dimethyl-2,2′-bipyridine) moiety.[23] Facile generation of single crystals for these complex classes would be of utmost importance for many research directions.

2. Experimental

2.1. General chemical procedures

All reactions were done using standard laboratory glassware. Ruthenium(III) trichloride hydrate was purchased from Johnson Matthey, 4,4′-dimethyl-2,2′-bipyridyl (≥99%) from Acros Organics, pentaamminechlorocobalt(III) chloride from Sigma Aldrich, 2,2′-bipyridyl from TCI Chemicals, acetone (≥99.8%) from Merck, dimethyl sulfoxide (DMSO, ≥99.5%), dichloromethane (DCM, ≥99%), ether (≥99%) from Sigma Aldrich, ethanol (≥99.8%) from VWR Chemicals. All chemicals were used without further purification. Solvents were of p.a. grade. Aluminum oxide 90 (basic) for column chromatography activity level 1 purchased from Macherey-Nagel was used for purification. *cis*-Ru(DMSO)$_4$Cl$_2$ was synthesized on a 2 mmol scale according to the literature in a yield of 69%.[24] The IR spectrum was recorded on a SpectrumTwo FT-IR Spectrometer (Perkin-Elmer) equipped with a Specac Golden Gate™ ATR accessory for neat samples. The frequencies are reported in wavenumbers (cm^{-1}).

Chromatography: Merck ALOX 60 (40–63 μm) with the indicated solvent system. Thin layer chromatography (TLC): Merck TLC plates silica gel 60 on aluminum with the indicated solvent system; the spots were visualized by UV light (254 and 366 nm). ^{1}H-NMR spectra were recorded on a Bruker AV-400 (400 MHz), the coupling constants are given in Hz. High-resolution electrospray mass spectra (HR-ESI-MS) were recorded on a maXis QTOF-MS instrument (Bruker Daltonics GmbH, Bremen, Germany). The samples were dissolved in a suitable solvent (*e.g.* MeOH) at a concentration of *ca.* 50 μg ml^{-1} and analyzed *via* continuous flow injection (2 μL min^{-1}). The mass spectrometer was operated in the positive electrospray ionization mode at 4000 V capillary voltage, −500 V endplate offset, with a N_2 nebulizer pressure of 0.8 bar and dry gas flow of 4 L min^{-1} at 180 °C. MS acquisitions were performed in the mass range from *m*/*z* 50 to 2000 at 20 000 resolution (full width at half maximum) and 1.0 Hz spectra rate. The mass analyzer was calibrated between *m*/*z* 118 and 2721 using an Agilent ESI-L low concentration tuning mix solution (Agilent, USA) at a resolution of 20 000 and a mass accuracy below 2 ppm. All solvents used were purchased in best LC-MS qualities. Elemental analyses were acquired on a LECO Truespec CHNS(O)-microanalyser. The used HPLC system was a VWR Hitachi Chromaster with a diode array detector 5430 and a ReproShell C_{18}, 2.6 μm, 75 × 4.6 mm column (Dr Maisch GmbH, Germany), which was kept at 40 °C. The used gradient was 95% A (water with 0.1% formic acid) and 5% B (acetonitrile) changing linearly within 5.8 minutes to 100% B, which was maintained for one minute. The aqueous solubilities of **1**

and **2** were determined by gravimetry and HPLC respectively. For **1**, 50 μL of a saturated solution of **1** were mixed together with 150 μL of water in order to dilute the solution enough for the lyophilization process. After lyophilization, the remaining weight of **1** was determined. In order to estimate the errors of this procedure, a similar experiment was done with 125 μL of a saturated sodium chloride solution. Based upon this and taking the concentration[25] and the density[26] of the saturated sodium chloride solution at 22 °C into account, the error of the gravimetric procedure was estimated to be 2%. For **2**, an aqueous saturated solution was diluted 540-fold. Its concentration was determined by comparing it with a calibration line, which was generated by 10-fold diluting an aqueous solution of 1.34 mg of **2** in 1 ml of water. Five different volumes between 1 and 20 μl of the 10-fold diluted solution of **2** were used to create the calibration line after manual integration. The error of the slope of the calibration line was calculated to be 0.5%. The HPLC procedure could not be applied to compound **1**, as it eluted too early together with the injection peak on our system.

2.2. Synthesis of the starting coordination complexes 1–3

Cobalt(III) tris(2,2′-bipyridine) chloride tris hydrate (1).[17] In a two-necked round bottom flask (10 mL), equipped with a magnetic stir bar, a septum and a reflux condenser, pentaamminechlorocobalt(III) chloride (79.5 mg, 0.32 mmol) was suspended in a 30% methanol–water solution (2 mL). 2,2′-Bipyridyl (148.4 mg, 0.95 mmol) was added and the purple suspension was heated to reflux (95 °C) until the TLC showed complete consumption of 2,2′-bipyridyl (8 hours). A clear orange brown solution was observed. The solvent was evaporated with a rotary evaporator after which the orange crude product was collected and further dried *in vacuo* (2 hours). The crude product was purified by thermal recrystallization. It was suspended in 3 mL EtOH and heated to 80 °C until a clear solution was observed. The clear orange solution was cooled to 23 °C and 1 mL of cyclohexane was added upon which a beige suspension was observed. The beige suspension was centrifuged. The mother liquor was removed, the beige solid collected and dried *in vacuo* to afford the desired product **1** as a beige solid (100 mg, 0.15 mmol) in a yield of 46%. Purity: >95% (^{1}H-NMR). TLC: R_f = 0.52 (MeOH/CH_2Cl_2 3 : 17). ^{1}H-NMR (D_2O): 8.82 (dd, J = 7.7, 1.0, 2 H); 8.53 (td, J = 7.8, 1.2, 2 H); 7.79–7.75 (m, 2 H); 7.45 (d, J = 6.0, 2 H). HR-ESI(+)-MS (H_2O): calc. for $[C_{30}H_{24}CoN_6]^{2+}$: 263.56910, exp.: 263.56917 (100%, Δ = 0.26 ppm); calc. for $[C_{20}H_{16}CoN_4]^{2+}$: 185.53480, exp.: 185.53461 (28%, Δ = 0.98 ppm), calc. for $[C_{30}H_{24}CoN_6]^{3+}$: 175.71260, exp.: 175.71252 (22%, Δ = 0.47 ppm). Anal. calcd for $[Co(bpy)_3]Cl_3{\cdot}5.5H_2O$: C, 49.16; H, 4.81; N, 11.47. Found: C, 48.74; H, 4.67; N, 11.93. The measured powder XRD pattern of **1** is shown in Fig. S3.† The aqueous solubility of **1** was determined by gravimetry to be 461 ± 9 mM.

Ruthenium(II) tris(4,4′-dimethyl-2,2′-bipyridine) chloride tetrahydrate (2).[18] *cis*-$Ru(DMSO)_4Cl_2$ [24] (0.64 g, 1.33 mmol) and 4,4′-dimethyl-2,2′-bipyridine (0.74 g, 4.02 mmol) were added to 25 mL of a 10% solution of water in ethylene glycol in a 100 mL round bottom flask equipped with a reflux condenser under the exclusion of light in N_2 atmosphere and heated to reflux (oil bath, 120 °C) for 1 hour. After cooling to room temperature, the orange solution was diluted with water (30 mL) and then a saturated solution of ammonium hexafluorophosphate salt (50 mL) was added until complete precipitation.[18a] The orange solid was filtered off and dried under reduced pressure to yield the hexafluorophosphate salt of **2** (97%, 1.22 g, 1.29 mmol) as orange crystals. IR (neat): 3595w, 2928w, 1620m, 1552w, 1479w, 1446w, 1304w, 1241w, 1038w, 988m, 972m, 821s. [Ru(II)(4,4′-dimethyl-2,2′-bipyridine)$_3$]Cl_2 (**2**) was synthesized as the tetrahydrate from the hexafluorophosphate salt on a 1.3 mmol scale according to the literature in a yield of 68%.[18a] Anal. calc. for $C_{36}H_{36}N_6RuCl_2(H_2O)_4$ (796.76): C 54.27, H 5.57, N 10.55, found: C 54.19, H 5.59, N 10.42. The aqueous solubility of **2** was determined by HPLC to be 309.4 ± 1.3 mM.

Preparation of [Co(II)(6,6″-(ethene-1,1-diyl)di-2,2′-bipyridine)(bromide)$_2$] (3). To a suspension of $MePPh_3Br$ (154 mg, 0.423 mmol, 1.43 eq.) in 4.5 mL THF was added KO*t*Bu (52.4 mg, 0.444 mmol, 1.5 eq.) in one portion and the resulting yellowish suspension was stirred for 1 hour at RT. Afterwards, di([2,2′-bipyridin]-6-yl)methanone[27] (100 mg, 0.296 mmol, 1.0 eq.) in 4 mL THF was added dropwise over a period of 10 minutes and the resulting brown solution was stirred for another 4 hours at RT. Upon full conversion, the reaction mixture was quenched with MeOH and diluted with water. The two phases were separated and the aqueous layer was extracted 3 times with DCM. The combined organic layers were dried over $MgSO_4$ and concentrated under reduced pressure to afford the crude product as a yellow oil. The crude product 6,6″-(ethene-1,1-diyl)di-2,2′-bipyridine was purified over basic ALOX (hexane/ethylacetate: 24 : 1) to afford 60.2 mg (61%) of the pure product as a white solid. ^{1}H NMR: (400 MHz, CD_3CN): 8.66 (ddd, J = 4.8, 1.7, 0.9, 2H); 8.41–8.34 (m, 4H); 7.89 (t, J = 7.9, 2H); 7.82 (td, J = 7.6, 1.9, 2H); 7.53 (dd, J = 7.7, 0.9, 2H); 7.36 (ddd, J = 7.5, 4.7, 1.2, 2H); 6.25 (s, 2H). HR-ESI (+)-MS: calc. for $[C_{22}H_{17}N_4]^+$: 337.14477, exp.: 337.14430.

To a solution of 6,6″-(ethene-1,1-diyl)di-2,2′-bipyridine (296 mg, 0.748 mmol, 1.0 eq.) in 12 mL acetonitrile was added $CoBr_2$ (155 mg, 0.711 mmol, 0.95 eq.) in one portion and the resulting red suspension was stirred for 3 hours at RT. The red precipitate was collected on a P3 glass filter frit and dried under HV for several hours to obtain 316 mg (76%) of the desired product **3** as a red solid. HR-ESI-MS: calc. for [M – 2Br]$^{2+}$: 197.53480, exp.: 197.53501. Anal. calcd for [Co(bpy$_2$CCH$_2$)Br$_2$]·1.5H_2O (%): C, 45.39; H, 3.29; N, 9.62. Found: C, 45.44; H, 3.26; N, 9.52.

2.3. Crystallographic procedures

The crystallization experiments were done as previously described[7a] using a Gryphon LCP nano-drop handler from Art Robbins Instruments in ARI Intelli-Plates 96-3 LVR. 500 nL of a stock solution of the cation to be crystallized (90% maximal saturation in water) were mixed with 500 nL of the stock solutions of the sodium and potassium salts and equilibrated against 75 μL of the stock solution of the same sodium or potassium salt *via* vapor diffusion. The screen contains 77

different sodium or potassium salts with a total of 96 different conditions and each coordination complex was tested for crystallization under those 96 conditions. The plates were incubated for 5–16 days at 20 °C. The Rock Imager 1000 took a picture of each well with normal light (immediately after setting up the plate and then after 2, 5, 10 and 16 days) and cross polarized light (immediately after setting up the plate and then after 5, 10 and 16 days).

Crystallographic data were collected at 160.0(1) K (with the exception of 100.00(11) K for **2b**) on a Rigaku OD XtaLAB Synergy Dualflex diffractometer equipped with a Pilatus 200 K detector and both PhotonJet Mo K_α and Cu K_α sources. Suitable crystals were covered with oil (Infineum V8512, formerly known as Paratone N), placed on a nylon loop that is mounted on a CrystalCap Magnetic™ pin (Hampton Research) and immediately transferred to the diffractometer. The program suite CrysAlis^{Pro} was used for data collection, numerical and multi-scan absorption correction as well as data reduction.[28] Each structure was solved with direct methods using ShelxT[29] and was refined by full-matrix least-squares methods on F^2 with SHELXL-2014[30] using the OLEX2 GUI.[31] Graphical output was produced with the help of the program Mercury[32] and the calculations of the geometry were done with the program Platon.[33] For **1a**, a 7 keV threshold was applied for the hybrid pixel Pilatus detector[34] in order to minimize the X-ray fluorescence caused by the cobalt complex being irradiated with copper radiation.[35] Additionally, the crystals of **1a** were twinned by a 180° rotation around the *a*-axis. The twin ratio was 69 : 31 and the two merged twin components were handled with the HKLF5 command in ShelxL. For **1c**, two complexes plus 15 water molecules and additional a half-occupied sodium chloride were found in the asymmetric unit, which corresponds to the unit cell (space group *P*1). Several water molecules were half occupied; their hydrogen atoms could not be found. One half occupied water molecule and a half-occupied sodium are located on the same position. Several restraints for the hydrogen atoms had to be used. For **2a**, the squeeze routine within Platon had to be used.[36] For **4c**, unexpectedly the spherical absorption correction was much better in terms of $I/\sigma(I)$ and R_{int} than the Gaussian or the numerical absorption correction. CCDC entries 1986517–1986525† contain the supplementary crystallographic data for this paper. Powder X-ray diffraction (PXRD) patterns were recorded on a STOE STADI P diffractometer equipped with a DECTRIS MYTHEN 1K detector in transmission mode using a Ge monochromator for Mo radiation (0.70930 Å).[37] Background correction of the recorded PXRD pattern was done with help of the software QUALX2.0.[38] Simulated PXRD pattern based on the single crystal analyses were generated with the help of the program Mercury.[32]

3. Results & discussion

The three chosen cationic (or cationic after anion dissociation), water-soluble metal complexes (**1–3**) were all subjected to the same high throughput screening Nano-Crystallization method,[7a] in which 500 nl of a 90% saturated aqueous solution of the complexes were mixed with 500 nl of an aqueous sodium salt solution containing the desired anion, which was added by a pipetting robot. Subsequently, this mixture was equilibrated by vapor diffusion against an excess of the same sodium salt solution. This procedure was repeated for each coordination complex with 95 different anion salt solutions to finally yield a completely filled 96-well crystallization plate with 96 different crystallization trials starting from one metal complex solution. The plates were incubated for 5–16 days at 20 °C in an imaging system. The Rock Imager 1000 took a picture of each well with normal light and cross polarized light. In the following, the results will be discussed for each obtained individual coordination complex moiety.

3.1 Crystallization of the cobalt(III) tris(2,2′-bipyridine) triscationic unit

Starting from cobalt(III) tris(2,2′-bipyridine) chloride, single crystals were obtained after mixing with either a 0.7 M solution of sodium dicyanamide, a 2.27 M solution of disodium DL-malate or a 2.92 M solution of disodium L-malate. All crystallographic data are summarized in Table S1.†

The aqueous mixture of cobalt(III) tris(2,2′-bipyridine) trichloride and sodium dicyanamide yielded crystals of cobalt(II) tris(2,2′-bipyridine) dicyanamide chloride·tetrahydrate (**1a**) in the hexagonal space group *P*6/*mcc* (Fig. 2). A 7 keV threshold was applied for the hybrid pixel Pilatus detector[34] in order to minimize the X-ray fluorescence caused by the cobalt complex being irradiated with copper radiation.[35] The cobalt center in **1a** was assigned without any doubt to be a Co(II), because the Co–N bond length in **1a** is 2.1259(16) Å. This value is perfectly in line with the range of Co(II)–N bond lengths between 2.117(8) and 2.141(7) Å in $[Co(II)(bpy)_3]Cl_2$.[39] On the other side, $[Co(III)(bpy)_3]Cl_3$ was reported to have Co–N bond lengths between 1.928(3)–1.939(3) Å.[22b] Synthetic experiments on a 0.4 mL scale revealed that the yield of this Co(II) complex is less than 10%. We postulate that the used dicyanamide anion is responsible for this reduction. The starting material cobalt(III) tris(2,2′-bipyridine) chloride (**1**) was analysed by elemental analysis and PXRD, but no signs for a cobalt(II) impurity could be found in **1**.

Single, red crystals of cobalt(III) bis(2,2′-bipyridine) DL-malate·decahydrate (**1b**) were obtained by vapor diffusion of a mixture of a 90% saturated solution of complex **1** and a 2.27 M solution of disodium DL-malate against a reservoir of a 2.27 M solution of disodium DL-malate. During crystallization a ligand exchange took place, whereby one 2,2′-bipyridine was replaced by a D- or L-malate anion. The resulting cobalt(III) bis(2,2′-bipyridine) DL-malate crystallized in the monoclinic space group *I*2/*a* (Fig. 2). The malate ligand coordinates as a bidentate trianion to the cobalt to yield a neutral complex overall. The substitution of one 2,2′-bipyridyl (bpy) (or the related 1,10-phenanthroline, phen) ligand within a cobalt(III)$(bpy)_3$ or cobalt(III)$(phen)_3$ complex by a dianionic α-hydroxycarboxylate has been reported before.[40]

Single, red crystals of cobalt(III) bis(2,2′-bipyridine) L-malate·9.25(H_2O)·0.25(NaCl) (**1c**) were obtained by vapor diffusion of a mixture of a 90% saturated solution of **1** and a

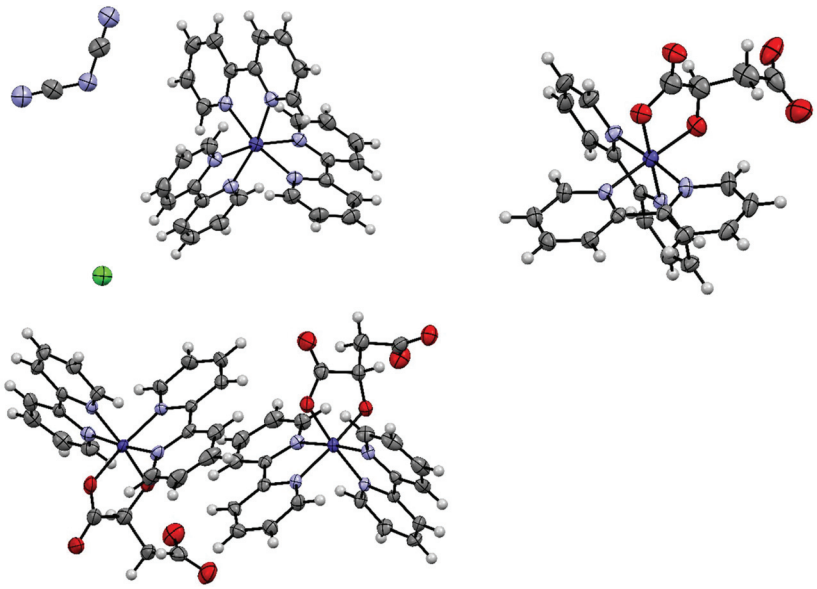

Fig. 2 Displacement ellipsoid representation of **1a** (top left), **1b** (top right) and **1c** (lower left). Ellipsoids are drawn at 50% probability. Disordered parts and water molecules are omitted for clarity.

2.92 M solution of disodium L-malate against a reservoir of a 2.92 M solution of disodium L-malate. Again, during crystallization a ligand exchange took place, whereby one 2,2′-bipyridine was replaced by one bidentate L-malate trianion. The resulting cobalt(III) bis(2,2′-bipyridine) L-malate crystallized in the triclinic, chiral space group *P*1. Both delta and lambda forms of cobalt(III) bis(2,2′-bipyridine) L-malate are present in the crystal in a 1 : 1 ratio.

In the crystallization trials leading to the red complexes **1b** and **1c**, additionally yellow crystals could be seen and were confirmed by single crystal analysis to be the already published crystal structure of starting material **1**.[22b] Microscope images of the two crystallization trials leading to compounds **1** as well as **1b** and **1c** respectively are shown in Fig. S6 and S8.†

3.2 Crystallization of the ruthenium(II) tris(4,4′-dimethyl-2,2′-bipyridine) dicationic unit

Single crystals containing the ruthenium(II) tris(4,4′-dimethyl-2,2′-bipyridine) dication were obtained from a mixture of a 90% saturated aqueous solution of ruthenium(II) tris(4,4′-dimethyl-2,2′-bipyridine) chloride and either a 0.73 M solution of disodium fumarate or a 1.57 M solution of sodium saccharinate. All crystallographic data are summarized in Table S2.†

The asymmetric unit of ruthenium(II) tris(4,4′-dimethyl-2,2′-bipyridine)·(hydrogenfumarate)·(hemifumarate)·(tetrahydrate) **2a** consists of one ruthenium(II) tris(4,4′-dimethyl-2,2′-bipyridine) dication, one hydrogenfumarate anion, half a fumarate dianion and four water molecules (Fig. 3). The asymmetric

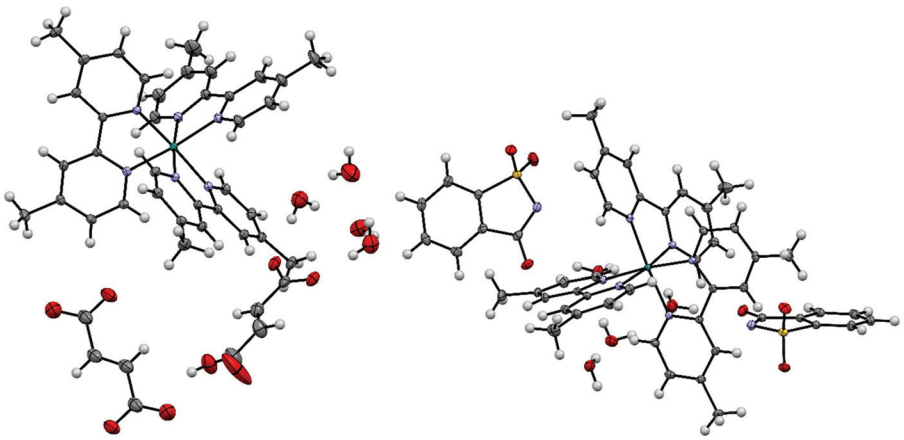

Fig. 3 Displacement ellipsoid representation of **2a** (left) and **2b** (right). Ellipsoids are drawn at 50% probability. An inversion center symmetry operation has been applied to form the complete fumarate anion. The smaller ellipsoids of **2b**, compared with the other structures, are caused by the lower measurement temperature of 100 K instead of 160 K.

unit in the case of **2b** consists of one ruthenium(II) tris(4,4′-dimethyl-2,2′-bipyridine) dication, two saccharinate anions and four water molecules. Compound **2b** was also synthesized on a macroscopic (0.13 mmol) scale from the chloride salt **2** with the help of an anion exchange column in a yield of 84% (see Chapter S5†).

3.3 Crystallization of the Co(II)(6,6″-(ethene-1,1-diyl)di-2,2′-bipyridine)(bromide)$_2$ (3) complex

The starting complex for the crystallizations was always cobalt(II) (6,6″-(ethene-1,1-diyl)di-2,2′-bipyridine)(bromide)$_2$ (**3**). We expected that one or two bromide ligands might dissociate, thereby yielding a cationic complex, which might be a suitable candidate for our Anion screen. Unexpectedly, all obtained crystal structures contained the cobalt(II) bis(2,2′-bipyrid-6′-yl) ketone dication. It seems that, when complex (**3**) is dissolved in water, its double bond is oxidatively cleaved under aerobic conditions, resulting in the carbonyl group at the bridging position of the products **4**. The hypothesis is supported by various publications, in which cobalt complexes are reported to catalyze the oxidative cleavage of terminal double bonds by molecular oxygen.[41] Single crystals containing the cobalt(II) bis(2,2′-bipyrid-6′-yl)ketone dication were obtained from a mixture of a 90% saturated aqueous solution of Co(II)(6,6″-(ethene-1,1-diyl)di-2,2′-bipyridine)(bromide)$_2$ and the same volume of either a 0.15 M solution of sodium *p*-toluenesulfonate (**4a**), a 0.725 M solution of disodium fumarate (**4b**), a 2 M solution of sodium tetrafluoroborate (**4c**) or a 0.06 M solution of disodium terephthalate (**4d**). All crystallographic data are summarized in Table S3.†

The asymmetric unit of **4a** contains a cobalt(II) bis(2,2′-bipyrid-6′-yl)ketone dication with an octahedral metal center coordinated by one *p*-toluenesulfonate anion and a water molecule. The remaining charge is compensated by a second free *p*-toluenesulfonate anion; additionally, there are four water molecules in the asymmetric unit (Fig. 4).

The asymmetric unit of **4b** contains a cobalt(II) bis(2,2′-bipyrid-6′-yl)ketone dication, one fumarate dianion and 2.25 water molecules (Fig. 4). The octahedral cobalt center is coordinated by the tetradendate ligand and two fumarate anions, where the latter bridge adjacent cobalt centers to form an infinite 1D-chain. The asymmetric unit of **4c** consists of one cobalt(II) bis(2,2′-bipyrid-6′-yl)ketone dication, two tetrafluoroborate anions and two water ligands (Fig. 5). The octahedral

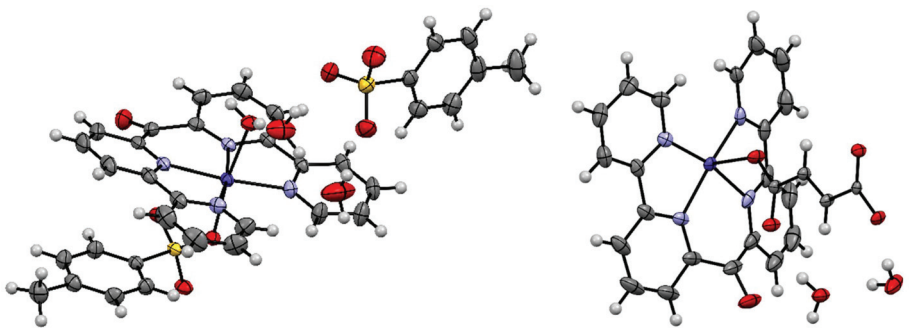

Fig. 4 Displacement ellipsoid representation of **4a** (left) and **4b** (right), ellipsoids drawn at 50% probability. One disordered water molecule in **4a** is omitted for clarity.

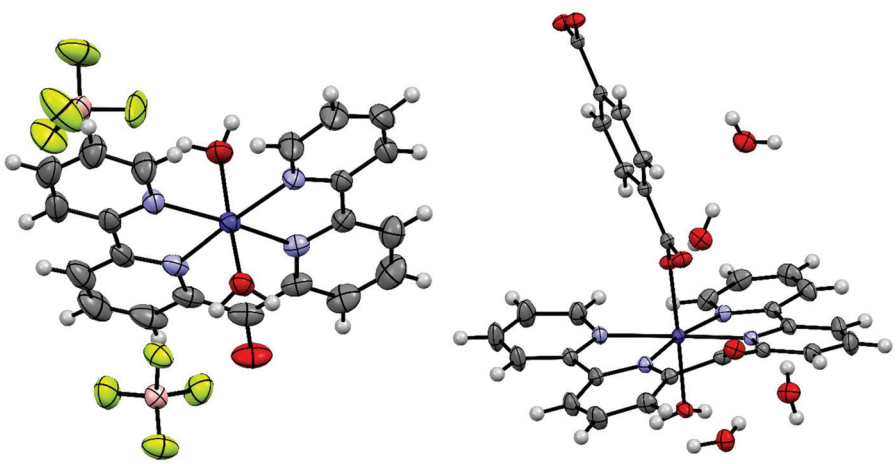

Fig. 5 Displacement ellipsoid representation of **4c** (left) and **4d** (right). Ellipsoids are drawn at 50% probability. For **4d**, the complete terephthalate ligand, which is created by a center of inversion, is shown for clarity. The free terephthalate dianion is omitted for clarity.

Table 1 Variation of metal to metal distances in cobalt(II) bis(2,2′-bipyrid-6′-yl)ketone complexes as a function of present anion, sorted by the shortest metal-to-metal distance. The anion vdW volumes were calculated with the help of the program MarvinSketch[43]

Compound	Anion	Shortest cobalt-to-cobalt distance	Axial metal coordination	Anion vdW volume [Å^3]	Ref.
4d	Terephthalate	6.8324(3)	Terephthalate bridged two cobalt metals, on the other side water that is bridged by one terephthalate to another water bound to Co	133	This work
4a	Tosylate	7.3475(3)	Tosylate on one side, water on the other	141	This work
4c	Tetrafluoroborate	7.9998(8)	Water molecules on both sides	54	This work
	Perchlorate	8.0982(9)	Water molecules on both sides	57	44
4b	Fumarate	8.1800(5)	Fumarate anions on both sides	88	This work
	Triflate	8.2128(7)	Triflate on both sides	85	27*a*

cobalt is coordinated by the ligand and two axially coordinated water molecules.

The asymmetric unit of **4d** consists of one cobalt(II) bis(2,2′-bipyrid-6′-yl)ketone dication with only half of the coordinated terephthalate ligand, one coordinated and three free water molecules and another half of a free terephthalate dianion (Fig. 5). Each terephthalate species sits on a center of inversion.

3.4 Variation of metal-to-metal distances caused by the presence of the different anions in six crystal structures containing the cobalt(II) bis(2,2′-bipyrid-6′-yl)ketone dication

The modulation of the metal-to-metal distance is of great importance for the magnetic properties in certain supramolecular molecular metal complexes.[42] Therefore, we asked ourselves, whether the Nano-Crystallization method could generate a diverse collection of coordination compounds that contain the same cationic metal complex with different anions. Each salt would be expected to have a different minimal metal-to-metal distance. Including this work, there are six crystal structures known that contain cobalt(II) complexes with the bis(2,2′-bipyrid-6′-yl)ketone ligand. This unique assembly of six coordination complexes, all having a N_4O_2 coordination environment, allows to study the influence of the introduced anion on the metal-to-metal distances (Table 1, see Table S4† for an extended listing of metal-to-metal distances). From the data, it is clear that the shortest metal-to-metal distance does not correlate with the vdW volume of the anions. The shortest cobalt-to-cobalt distance among all six studied compounds, in **4d**, is present between neighboring complexes, which are not bridged by any ligand. The second shortest distance, in **4a**, is between two cobalt centers, which are bridged by an aqua ligand, which makes one hydrogen bond to a κ*O*:κ*O*′ bridging sulfonate group of the tosylate anion, that is coordinating to the next cobalt center.

4. Conclusion

For all three tested metal coordination complexes, the Nano-Crystallization method was able to generate novel single crystal structures with different anions, in which at least one of the original halide anions was replaced. This method can be recommended for cationic coordination complexes, which are stable in water and have an aqueous solubility of at least 2 mM. The shortest metal-to-metal distance was found to be purely dependent upon the interaction of the anion within the crystalline lattice and not upon the vdW size of the anion (Table 1).

Conflicts of interest

The University of Zurich has a license agreement with Molecular Dimensions Ltd, which states that Molecular Dimension Ltd has the right to sell the Anion Screen.

Acknowledgements

We thank the University of Zurich and the R'Equip programme of the Swiss National Science Foundation (project no. 206021_164018) for financial support. We thank Esmael Balaghi for measuring the PXRD, Viviane Grange for measuring the elemental analyses, Franziska Rahn and Matthias Berchtold for help with the HPLC measurements and Prof. Dr Anthony Linden for a critical reading of the manuscript.

References

1 (*a*) B. Spingler, S. Schnidrig, T. Todorova and F. Wild, *CrystEngComm*, 2012, **14**, 751–757; (*b*) P. P. Nievergelt and B. Spingler, *CrystEngComm*, 2017, **19**, 142–147.

2 (*a*) H.-H. Tung, E. L. Paul, M. Midler and J. A. McCauley, *Crystallization of Organic Compounds: An Industrial Perspective*, John Wiley & Sons, Inc., 2009; (*b*) R. J. Davey, S. L. Schroeder and J. H. ter Horst, *Angew. Chem., Int. Ed.*, 2013, **52**, 2166–2179; (*c*) Y. Tamura, H. Takezawa, Y. Domoto and M. Fujita, *Chem. Lett.*, 2018, **47**, 617–619; (*d*) N. Wada, R. D. Kersten, T. Iwai, S. Lee, F. Sakurai, T. Kikuchi, D. Fujita, M. Fujita and J. K. Weng, *Angew. Chem., Int. Ed.*, 2018, **57**, 3671–3675; (*e*) A. Tyler, R. Ragbirsingh, C. McMonagle, P. Waddell, S. Heaps, J. Steed, P. Thaw, M. Hall and M. Probert, *ChemRxiv*, 2019, 11366054.

3 (*a*) I. A. Ibarra, P. A. Bayliss, E. Pérez, S. Yang, A. J. Blake, H. Nowell, D. R. Allan, M. Poliakoff and M. Schröder, *Green Chem.*, 2012, **14**, 117–122; (*b*) P. A. Bayliss, I. A. Ibarra, E. Pérez, S. Yang, C. C. Tang, M. Poliakoff and M. Schröder, *Green Chem.*, 2014, **16**, 3796–3802; (*c*) B. Saccoccia, A. M. Bohnsack, N. W. Waggoner, K. H. Cho, J. S. Lee, D.-Y. Hong, V. M. Lynch, J.-S. Chang and S. M. Humphrey, *Angew. Chem., Int. Ed.*, 2015, **54**, 5394–5398; (*d*) K. Sumida, K. Liang, J. Reboul, I. A. Ibarra, S. Furukawa and P. Falcaro, *Chem. Mater.*, 2017, **29**, 2626–2645.

4 (*a*) E. Biemmi, S. Christian, N. Stock and T. Bein, *Microporous Mesoporous Mater.*, 2009, **117**, 111–117; (*b*) P. J. Kitson, R. J. Marshall, D. Long, R. S. Forgan and L. Cronin, *Angew. Chem., Int. Ed.*, 2014, **53**, 12723–12728; (*c*) M. L. Kelty, W. Morris, A. T. Gallagher, J. S. Anderson, K. A. Brown, C. A. Mirkin and T. D. Harris, *Chem. Commun.*, 2016, **52**, 7854–7857; (*d*) S. M. Moosavi, A. Chidambaram, L. Talirz, M. Haranczyk, K. C. Stylianou and B. Smit, *Nat. Commun.*, 2019, **10**, 539.

5 C. G. Jones, M. Asay, L. J. Kim, J. F. Kleinsasser, A. Saha, T. J. Fulton, K. R. Berkley, D. Cascio, A. G. Malyutin, M. P. Conley, B. M. Stoltz, V. Lavallo, J. A. Rodríguez and H. M. Nelson, *ACS Cent. Sci.*, 2019, **5**, 1507–1513.

6 R. Taylor and P. A. Wood, *Chem. Rev.*, 2019, **119**, 9427–9477.

7 (*a*) P. P. Nievergelt, M. Babor, J. Čejka and B. Spingler, *Chem. Sci.*, 2018, **9**, 3716–3722; (*b*) M. Babor, P. P. Nievergelt, J. Čejka, V. Zvoníček and B. Spingler, *IUCrJ*, 2019, **6**, 145–151.

8 R. Bolliger, A. Frei, H. Braband, G. Meola, B. Spingler and R. Alberto, *Chem. – Eur. J.*, 2019, **25**, 7101–7104.

9 W.-H. Jiang, H.-Z. Zhang, G.-F. Hou, D.-S. Ma, B. Liu and Y.-H. Yu, *RSC Adv.*, 2017, **7**, 45641–45651.

10 (*a*) P. Diaz, J. Benet-Buchholz, R. Vilar and A. J. P. White, *Inorg. Chem.*, 2006, **45**, 1617–1626; (*b*) I. A. Koval, M. Sgobba, M. Huisman, M. Lüken, E. Saint-Aman, P. Gamez, B. Krebs and J. Reedijk, *Inorg. Chim. Acta*, 2006, **359**, 4071–4078; (*c*) J. Suárez-Varela, A. J. Mota, H. Aouryaghal, J. Cano, A. Rodriguez-Diéguez, D. Luneau and E. Colacio, *Inorg. Chem.*, 2008, **47**, 8143–8158; (*d*) P. Mukherjee, M. G. B. Drew, M. Estrader, C. Diaz and A. Ghosh, *Inorg. Chim. Acta*, 2008, **361**, 161–172; (*e*) L. Botana, J. Ruiz, J. M. Seco, A. J. Mota, A. Rodríguez-Diéguez, R. Sillanpää and E. Colacio, *Dalton Trans.*, 2011, **40**, 12462–12471; (*f*) R. A. Polunin, K. S. Gavrilenko, M. A. Kiskin, I. L. Eremenko, V. M. Novotortsev and S. V. Kolotilov, *Russ. J. Coord. Chem.*, 2016, **42**, 487–493.

11 (*a*) J. Fielden, P. T. Gunning, D.-L. Long, M. Nutley, A. Ellern, P. Kögerler and L. Cronin, *Polyhedron*, 2006, **25**, 3474–3480; (*b*) R. Mondal, T. Basu, D. Sadhukhan, T. Chattopadhyay and M. K. Bhunia, *Cryst. Growth Des.*, 2009, **9**, 1095–1105.

12 (*a*) A. N. Khlobystov, A. J. Blake, N. R. Champness, D. A. Lemenovskii, A. G. Majouga, N. V. Zyk and M. Schröder, *Coord. Chem. Rev.*, 2001, **222**, 155–192; (*b*) X. Li, Y. Gong, H. Zhao and R. Wang, *Inorg. Chem.*, 2014, **53**, 12127–12134.

13 X.-R. Meng, X.-J. Wu, D.-W. Li, H.-W. Hou and Y.-T. Fan, *Polyhedron*, 2010, **29**, 2619–2628.

14 Y. Mu, Y. Zhao, H. Xu, H. Hou and Y. Fan, *J. Mol. Struct.*, 2009, **935**, 144–150.

15 P. Chen, M. Zhang, W. Sun, H. Li, L. Zhao and P. Yan, *CrystEngComm*, 2015, **17**, 5066–5073.

16 V. Bugris, C. Dudás, B. Kutus, V. Harmat, K. Csankó, S. Brockhauser, I. Pálinkó, P. Turner and P. Sipos, *Acta Crystallogr., Sect. B: Struct. Sci., Cryst. Eng. Mater.*, 2018, **74**, 598–609.

17 N. Maki, *Bull. Chem. Soc. Jpn.*, 1969, **42**, 2275–2281.

18 (*a*) J. Lacour, C. Goujon-Ginglinger, S. Torche-Haldimann and J. J. Jodry, *Angew. Chem., Int. Ed.*, 2000, **39**, 3695–3697; (*b*) A. M. Todd, A. N. Swinburne, A. E. Goeta and J. W. Steed, *New J. Chem.*, 2013, **37**, 89–96.

19 (*a*) J. T. Kirner and C. M. Elliott, *J. Phys. Chem. C*, 2015, **119**, 17502–17514; (*b*) O. S. Wenger, *Coord. Chem. Rev.*, 2015, **282**, 150–158.

20 (*a*) S. Aghazada and M. K. Nazeeruddin, *Inorganics*, 2018, **6**, 52; (*b*) A. Colombo, C. Dragonetti, A. Valore, C. Coluccini, N. Manfredi and A. Abbotto, *Polyhedron*, 2014, **82**, 50–56.

21 S. Aghazada, I. Zimmermann, Y. M. Ren, P. Wang and M. K. Nazeeruddin, *ChemistrySelect*, 2018, **3**, 1585–1592.

22 (*a*) M. Du, X.-J. Zhao and H. Cai, *Z. Kristallogr. – New Cryst. Struct.*, 2004, **219**, 463–465; (*b*) W. Liu, W. Xu, J.-L. Lin and H.-Z. Xie, *Acta Crystallogr., Sect. E: Struct. Rep. Online*, 2008, **64**, m1586–m1586.

23 (*a*) T. J. Rutherford, P. A. Pellegrini, J. Aldrich-Wright, P. C. Junk and F. R. Keene, *Eur. J. Inorg. Chem.*, 1998, 1677–1688; (*b*) J. Karges, O. Blacque, P. Goldner, H. Chao and G. Gasser, *Eur. J. Inorg. Chem.*, 2019, **2019**, 3704–3712.

24 I. Bratsos, E. Alessio, M. E. Ringenberg and T. B. Rauchfuss, *Inorg. Synth.*, 2010, **35**, 148–152.

25 R. W. Potter II and M. A. Clynne, *J. Res. U.S. Geol. Surv.*, 1978, **6**, 701–705.

26 V. L. Thurmond, R. W. Potter II and M. A. Clynne, *The densities of saturated solutions of NaCl and KCl from 10 °C to 105 °C*, U. S. Geological Survey, 1984.

27 (*a*) S. Schnidrig, C. Bachmann, P. Müller, N. Weder, B. Spingler, E. Joliat-Wick, M. Mosberger, J. Windisch, R. Alberto and B. Probst, *ChemSusChem*, 2017, **10**, 4570–4580; (*b*) H. Nierengarten, J. Rojo, E. Leize, J.-M. Lehn and A. Van Dorsselaer, *Eur. J. Inorg. Chem.*, 2002, 573–579.

28 *Rigaku Oxford Diffraction, CrysAlisPro Software system 1.171.40*, Rigaku Corporation, 2018.

29 G. M. Sheldrick, *Acta Crystallogr., Sect. A: Found. Adv.*, 2015, **71**, 3–8.

30 G. M. Sheldrick, *Acta Crystallogr., Sect. C: Struct. Chem.*, 2015, **71**, 3–8.

31 O. V. Dolomanov, L. J. Bourhis, R. J. Gildea, J. A. K. Howard and H. Puschmann, *J. Appl. Crystallogr.*, 2009, **42**, 339–341.

32 C. F. Macrae, L. Sovago, S. J. Cottrell, P. T. A. Galek, P. McCabe, E. Pidcock, M. Platings, G. P. Shields,

J. S. Stevens, M. Towler and P. A. Wood, *J. Appl. Crystallogr.*, 2020, **53**, 226–235.
33 A. L. Spek, *Acta Crystallogr., Sect. D: Biol. Crystallogr.*, 2009, **65**, 148–155.
34 (*a*) P. Kraft, A. Bergamaschi, C. Broennimann, R. Dinapoli, E. F. Eikenberry, B. Henrich, I. Johnson, A. Mozzanica, C. M. Schlepütz, P. R. Willmott and B. Schmitt, *J. Synchrotron Radiat.*, 2009, **16**, 368–375; (*b*) C. Brönnimann and P. Trüb, in *Synchrotron Light Sources and Free-Electron Lasers: Accelerator Physics, Instrumentation and Science Applications*, ed. E. J. Jaeschke, S. Khan, J. R. Schneider and J. B. Hastings, Springer International Publishing, Cham, 2016, pp. 995–1027; (*c*) A. Förster, S. Brandstetter and C. Schulze-Briese, *Philos. Trans. R. Soc., A*, 2019, **377**, 20180241.
35 L. Prieto, M. Neuburger, B. Spingler and F. Zelder, *Org. Lett.*, 2016, **18**, 5292–5295.
36 A. L. Spek, *Acta Crystallogr., Sect. C: Struct. Chem.*, 2015, **71**, 9–18.
37 S. E. Balaghi, C. A. Triana and G. R. Patzke, *ACS Catal.*, 2020, **10**, 2074–2087.
38 A. Altomare, N. Corriero, C. Cuocci, A. Falcicchio, A. Moliterni and R. Rizzi, *J. Appl. Crystallogr.*, 2015, **48**, 598–603.
39 D. J. Szalda, C. Creutz, D. Mahajan and N. Sutin, *Inorg. Chem.*, 1983, **22**, 2372–2379.
40 (*a*) R. A. Haines and D. W. Bailey, *Inorg. Chem.*, 1975, **14**, 1310–1312; (*b*) A. Tatehata, *Inorg. Chem.*, 1976, **15**, 2086–2090.
41 (*a*) R. S. Drago, B. B. Corden and C. W. Barnes, *J. Am. Chem. Soc.*, 1986, **108**, 2453–2454; (*b*) Y. H. Lin, I. D. Williams and P. Li, *Appl. Catal., A*, 1997, **150**, 221–229; (*c*) X. Zhou and H. Ji, *Chin. J. Chem.*, 2012, **30**, 2103–2108; (*d*) B. Biannic and J. J. Bozell, *Org. Lett.*, 2013, **15**, 2730–2733.
42 (*a*) M. Atzori, A. Serpe, P. Deplano, J. A. Schlueter and M. L. Mercuri, *Inorg. Chem. Front.*, 2015, **2**, 108–115; (*b*) V. V. Lukov, I. N. Shcherbakov, S. I. Levchenkov, Y. P. Tupolova, L. D. Popov, I. V. Pankov and S. V. Posokhova, *Russ. J. Coord. Chem.*, 2019, **45**, 163–187.
43 ChemAxon Ltd., *MarvinSketch 20.6*, 2020.
44 J. C. Knight, A. J. Amoroso, P. G. Edwards, R. Prabaharan and N. Singh, *Dalton Trans.*, 2010, **39**, 8925–8936.

Supporting information for

Single crystal growth of water-soluble metal complexes with the help of the Nano-Crystallization method

Ricardo Alvarez, Philipp Nievergelt, Ekaterina Slyshkina, Peter Müller, Roger Alberto, Bernhard Spingler*

Department of Chemistry, University of Zurich, 8057 Zurich, Switzerland

* Corresponding author: spingler@chem.uzh.ch

Figure S1 ^{1}H-NMR (D_2O) of cobalt(III) tris(2,2'-bipyridine) chloride (**1**).

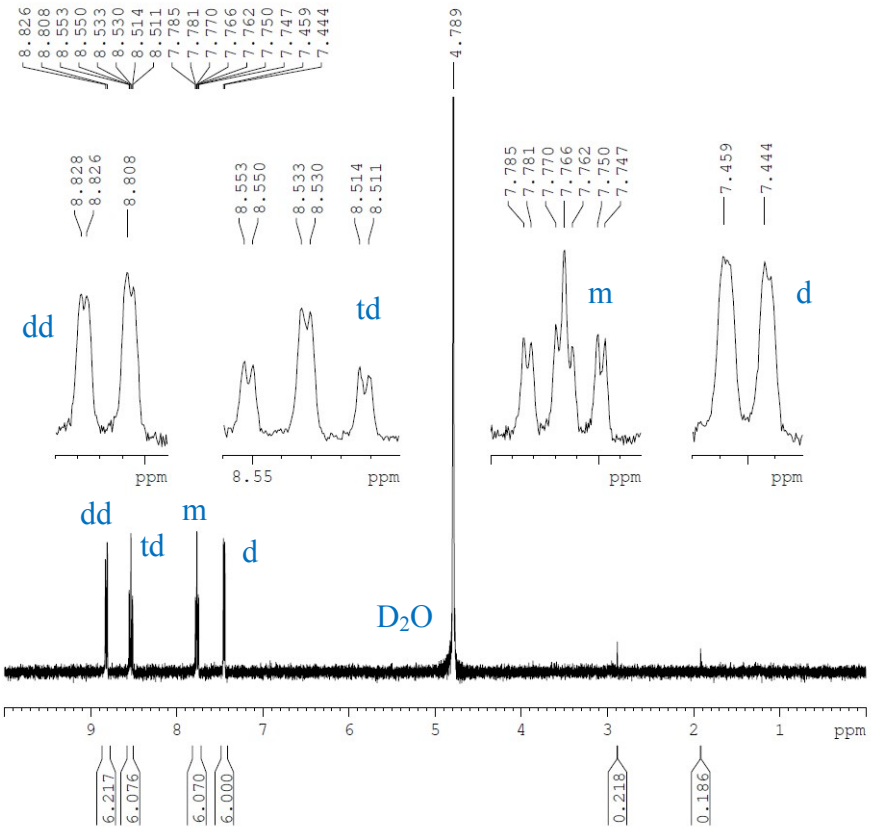


```
Current Data Parameters
NAME                  PN4-2-2
EXPNO                       1
PROCNO                      1

F2 - Acquisition Parameters
Date_              20180911
Time                   11.38
INSTRUM                spect
PROBHD    5 mm PAQNP Swi
PULPROG                zg30
TD                    65536
SOLVENT                 D2O
NS                       16
DS                        2
SWH               12335.526 Hz
FIDRES             0.188225 Hz
AQ                2.6563926 sec
RG                      406
DW                   40.533 usec
DE                    6.50 usec
TE                   298.1 K
D1               3.00000000 sec
TD0                         1

======== CHANNEL f1 ========
SFO1           400.1324008 MHz
NUC1                     1H
P1                    12.60 usec
PLW1           15.84899998 W

F2 - Processing parameters
SI                    65536
SF               400.1299641 MHz
WDW                      EM
SSB          0
LB           0 Hz
GB           0
PC                     1.00
```

Figure S2 Simulated powder pattern of $[Co(III)(bpy)_3]Cl_3 \cdot 4(H_2O)$ (**1**) with help of the Mercury software[1] based on the single crystal structure of **1**.

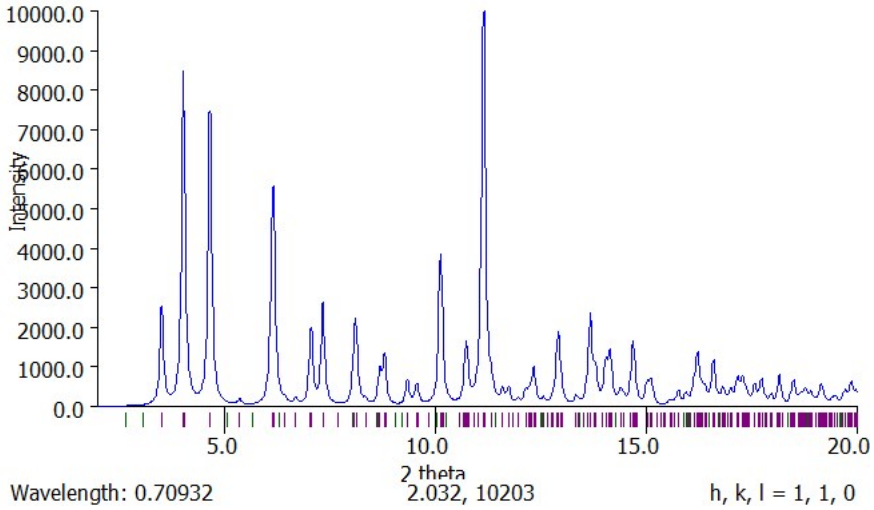

Figure S3 Measured PXRD pattern of **1**.

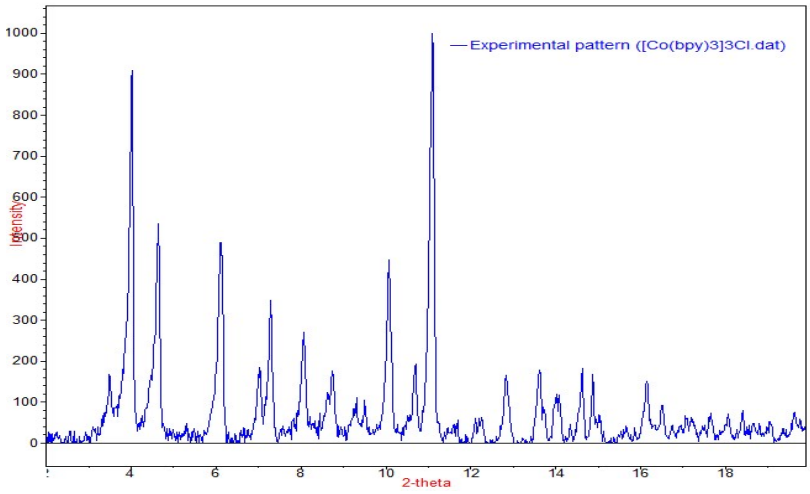

S1 Cobalt(II) tris(2,2'-bipyridine) dicyanamide chloride · tetrahydrate (1a)

Single crystals of **1a** were obtained with help of the high throughput screening method for nano-crystallization of salts by vapor diffusion at 20 °C of 500 nL of a 90% saturated solution of **1** in water mixed with the same volume of a 0.7 M solution of sodium dicyanamide against a reservoir of a 0.7 M solution of sodium dicyanamide. The crystallographic data are summarized in Table S1. In order to minimize the X-ray fluorescence caused by the cobalt complex being irradiated with copper radiation[2], a 7 keV threshold was applied for the hybrid pixel Pilatus detector.[3] **1a** crystallized in the hexagonal space group *P*6/mcc. The tris-bipyridine cobalt(II) cation and the dicyanamide are both sitting on a three-fold symmetry axis (Figure 1). The two cyano groups of the dicyanamide and one water molecule occupy common positions and are therefore disordered in a ratio 67:33.

Figure S4 Packing diagram of **1a**.

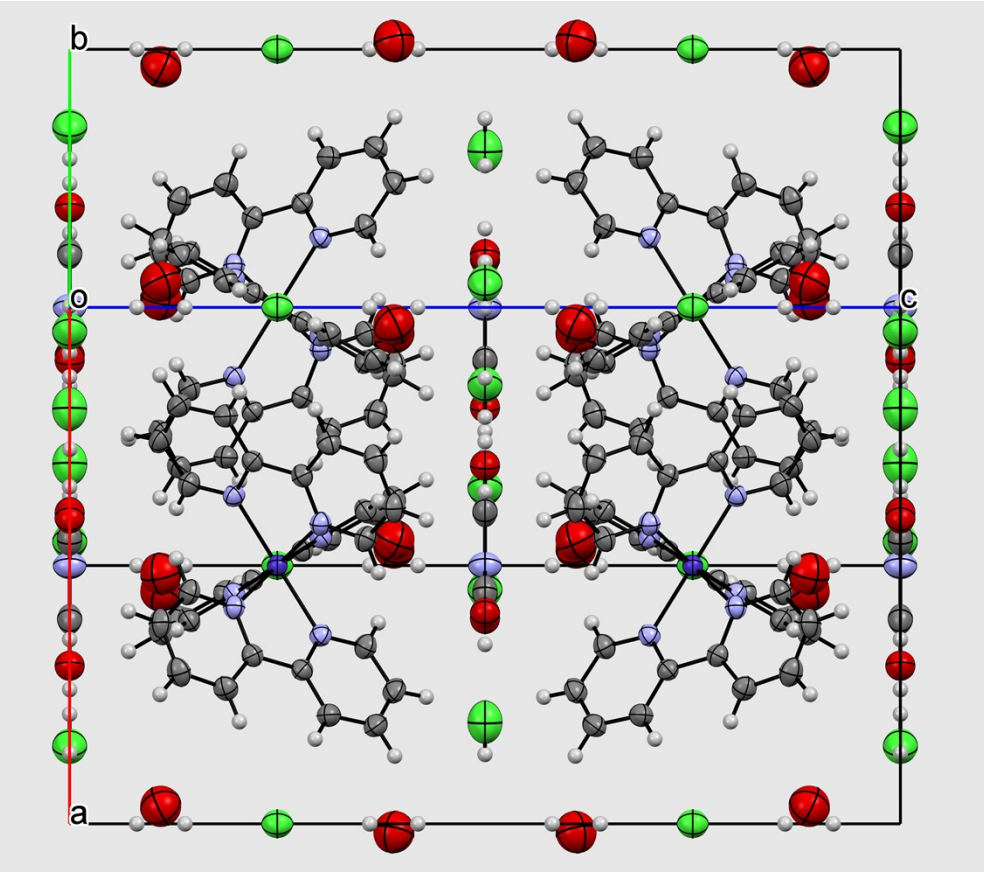

S2 Cobalt(III) bis(2,2'-bipyridine) DL-malate · 10 hydrate (1b)

Single, red crystals of **1b** were obtained from the high throughput screening method for nano-crystallization of salts by vapor diffusion at 20°C of 500 nL of a 90% saturated solution of **1** in water mixed with the same volume of a 2.27 M solution of disodium DL-malate against a reservoir of a 2.27 M solution of disodium DL-malate. The crystallographic data are summarized in Table S1. During crystallization a ligand exchange took place in which one 2,2'-bipyridine ligand was replaced by a D- or L-malate anion. The resulting cobalt(III) bis(2,2'-bipyridine) DL-malate crystallized in the monoclinic space group *I*2/a. The asymmetric unit consists of half a molecule of cobalt(III) bis(2,2'-bipyridine) malate and 5 water molecules. The other half of the molecule is generated by the two-fold rotational axis of the space group, which passes through the Co-atom and the malate ligand, thereby indicating that part of the malate ligand is disordered. The D- and L-malate are coordinated as a bidentate trianion to the cobalt. The neighboring water molecule are disordered in a ratio of 50:50.

Additionally to **1b**, the crystallization also yielded the known yellow crystals of the starting material cobalt(III) tris(2,2'-bipyridine) chloride tetrahydrate (**1**)[4] (Figure S6).

Figure S5 Packing diagram of **1b**.

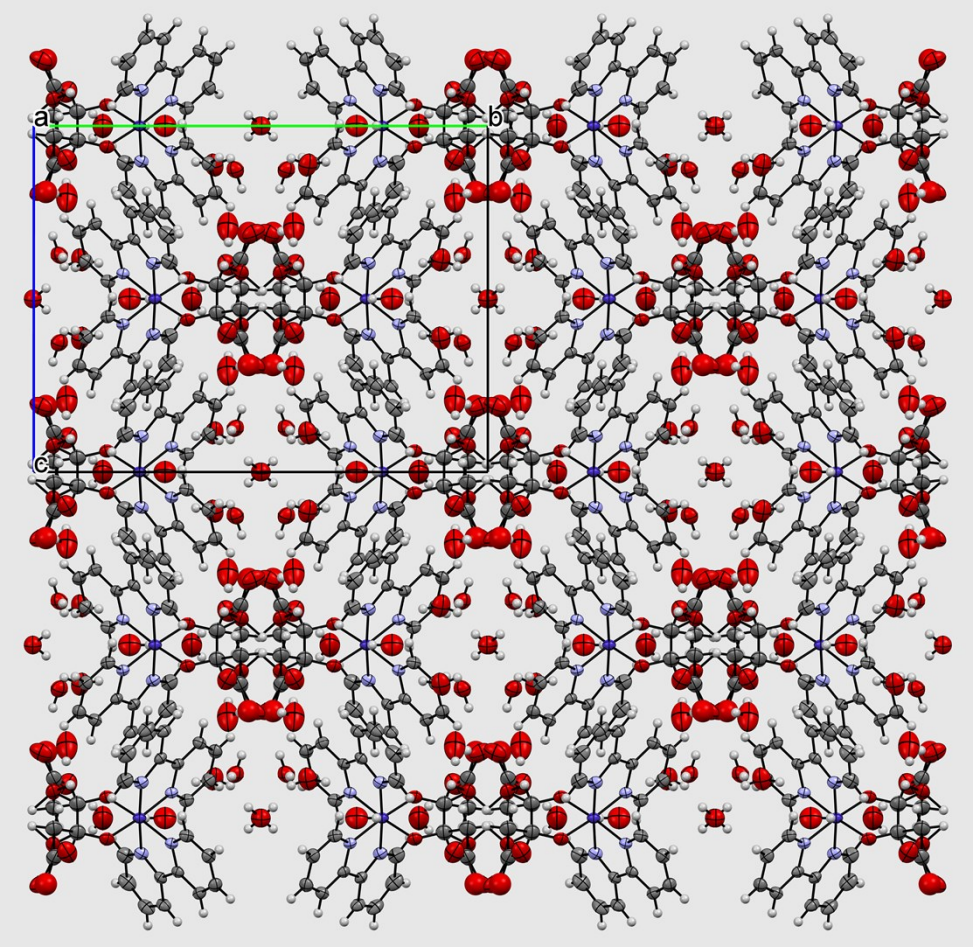

Figure S6 Crystallization of red **1c** and yellow **1** in a 36 µL sitting drop.

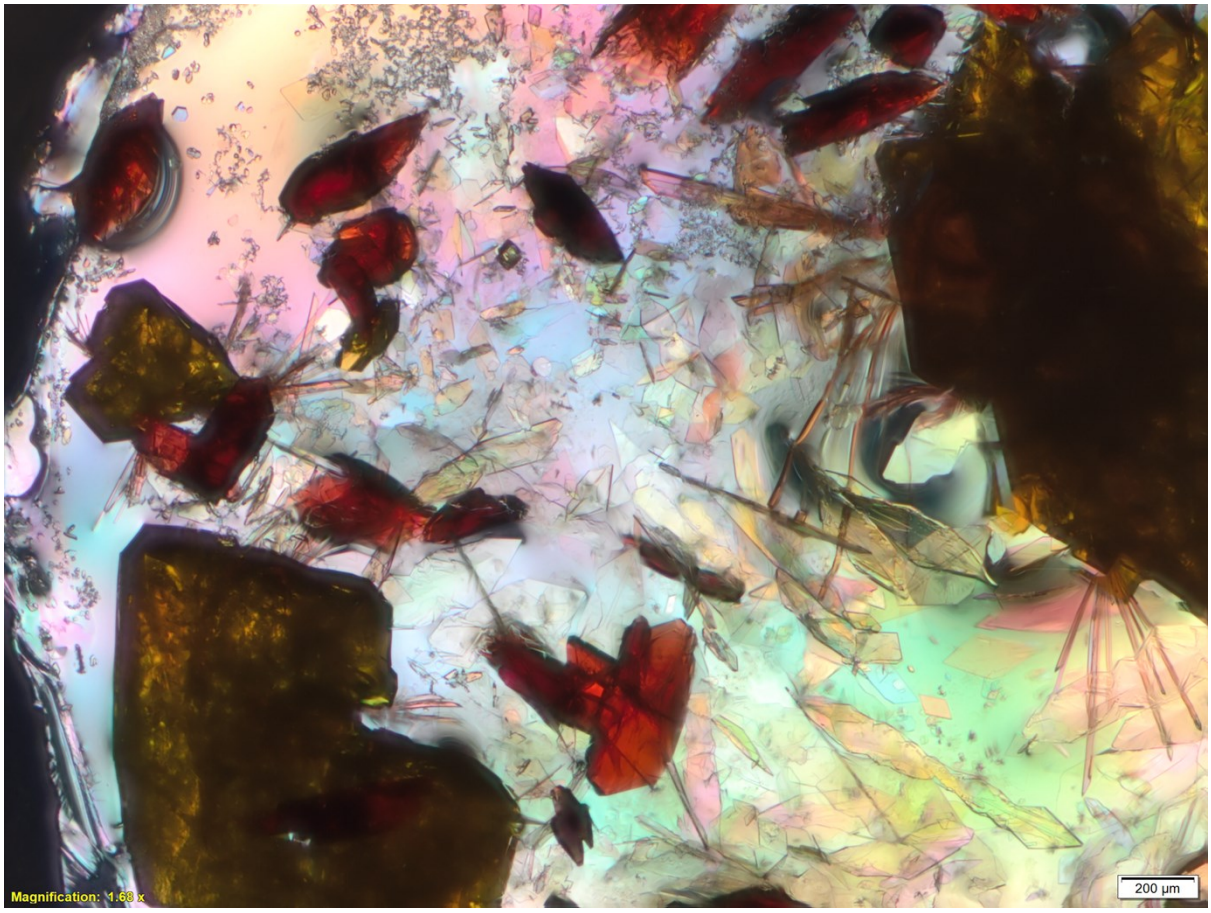

S3 Cobalt(III) bis(2,2'-bipyridine) L-malate · 9.25 hydrate · 0.25 sodium chloride (1c)

Single, red crystals were obtained from the high throughput screening method for nano-crystallization of salts by vapor diffusion at 20 °C of 500 nL of a 90% saturated solution of **1** in water mixed with the same volume of a 2.92 M solution of disodium L-malate against a reservoir of a 2.92 M solution of disodium L-malate. The crystallographic data are summarized in Table S1. During crystallisation a ligand exchange took place whereby one 2,2'-bipyridine ligand was replaced with one trianionic L-malate molecule. The resulting cobalt(III) bis(2,2'-bipyridine) L-malate crystallised in the triclinic, chiral space group P1. The asymmetric unit consists of one delta and one lambda molecule of cobalt(III) bis(2,2'-bipyridine) L-malate, half a chloride anion, half a sodium cation and 18.5 water molecules. A half-occupied water molecule and the half-occupied chloride anion occupy the same crystallographic site.

Additionally to **1c**, the crystallization also yielded the known yellow crystals of the starting material cobalt(III) tris(2,2'-bipyridine) chloride tetrahydrate (**1**)[4] (Figure S8). Repeating the crystallization experiment with a 2.27 M L-malate solution (same malate concentration as used with DL-malate for the crystallization of **1b**) yielded again both complexes (Figure S9).

Figure S7 Packing diagram of **1c**.

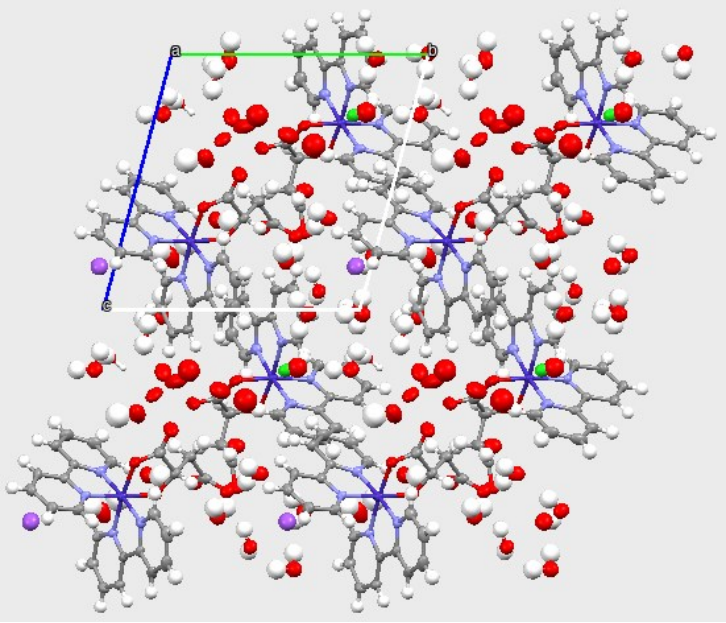

Figure S8 Crystallization of red **1c** and yellow **1** in a 36 µL sitting drop.

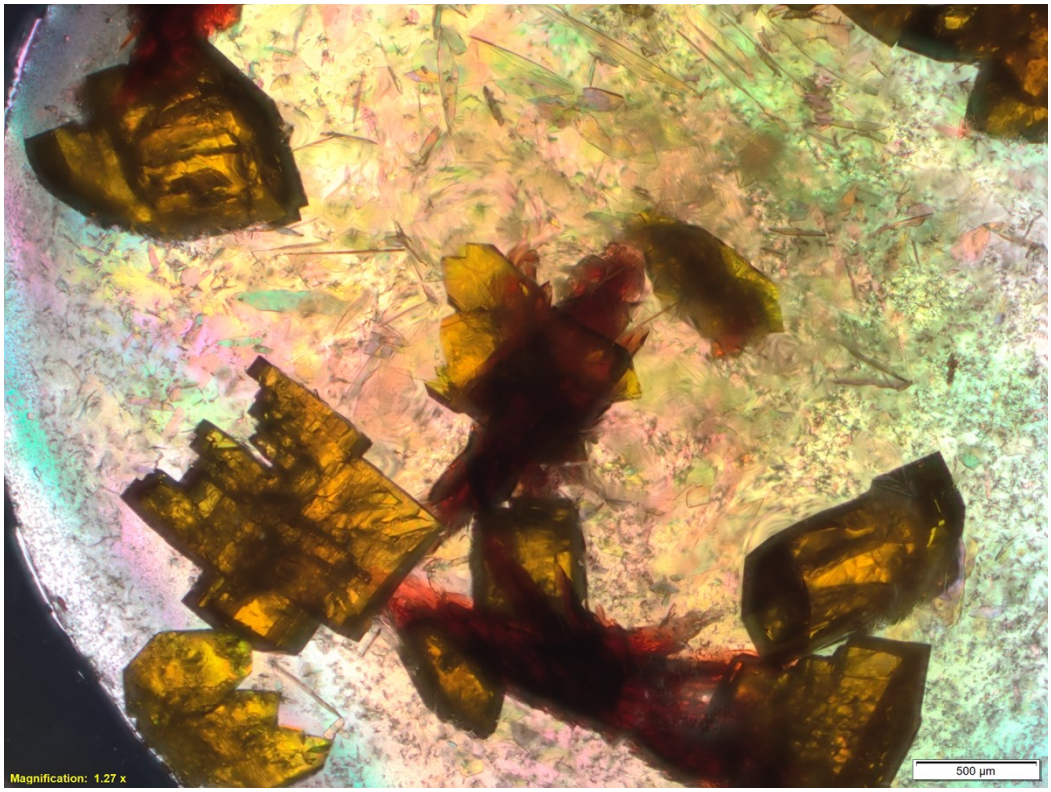

Figure S9 Crystallization of red **1c** and yellow **1** in a 36 µL sitting drop using a 2.27 M L-malate solution.

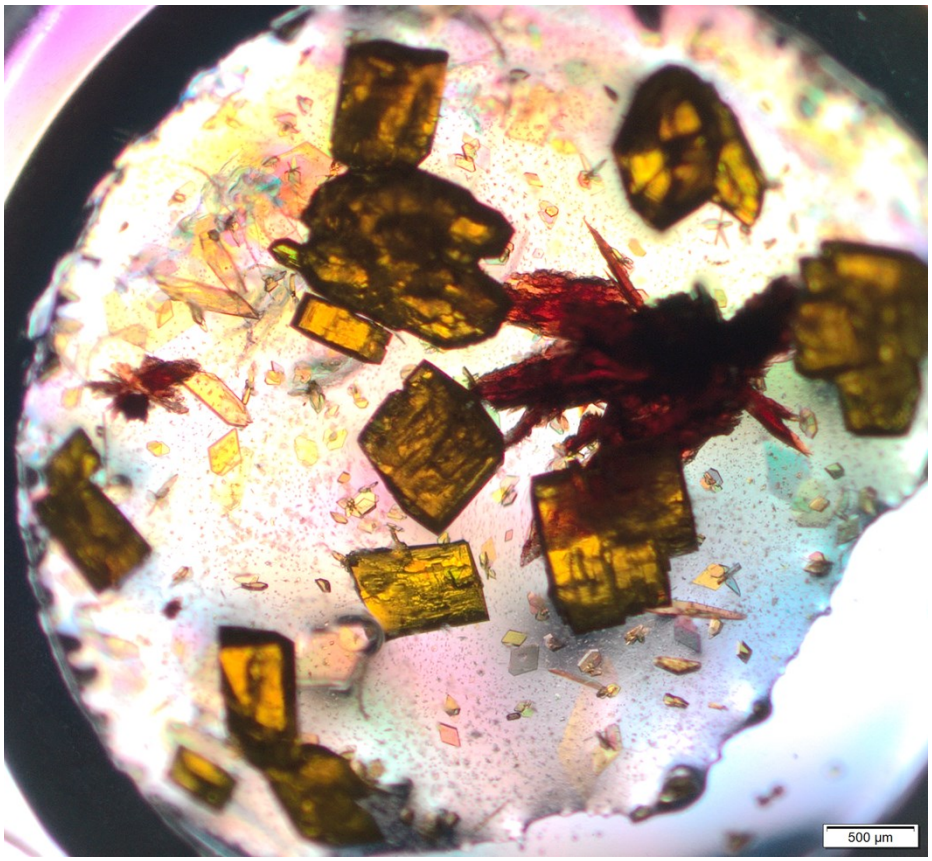

S4 Ruthenium(II) tris(4,4'-dimethyl-2,2'-bipyridine) hydrogenfumarate hemifumarate tetrahydrate (2a)

Single crystals of **2a** were obtained from the high throughput screening method for nano-crystallization of salts by vapor diffusion at 20°C of 500 nL of a 90% saturated solution of **2** in water mixed with the same volume of a 0.73 M solution of disodium fumarate against a reservoir of a 0.73 M solution of disodium fumarate. The crystallographic data are summarized in Table S2. **2a** crystallized in the monoclinic space group $P2_1/n$. The asymmetric unit consists of one ruthenium(II) tris(4,4'-dimethyl-2,2'-bipyridine) cation, one hydrogenfumarate anion, half a fumarate dianion, which sits across an inversion center, and four water molecules. The remaining ill-defined electron density had to be treated with the SQUEEZE procedure within *Platon*.[5]

Macroscopic synthesis of **2a** was done by vapor diffusion at 20°C of 200 µL of a 90% saturated solution of **2** in water mixed with the same volume of a 0.73 M solution of disodium fumarate against 1.8 mL of a 0.73 M solution of disodium fumarate. The obtained material was analysed by PXRD (Figure S12), it mainly contained **2a** but also an unknown impurity.

Figure S10 Packing diagram of **2a**.

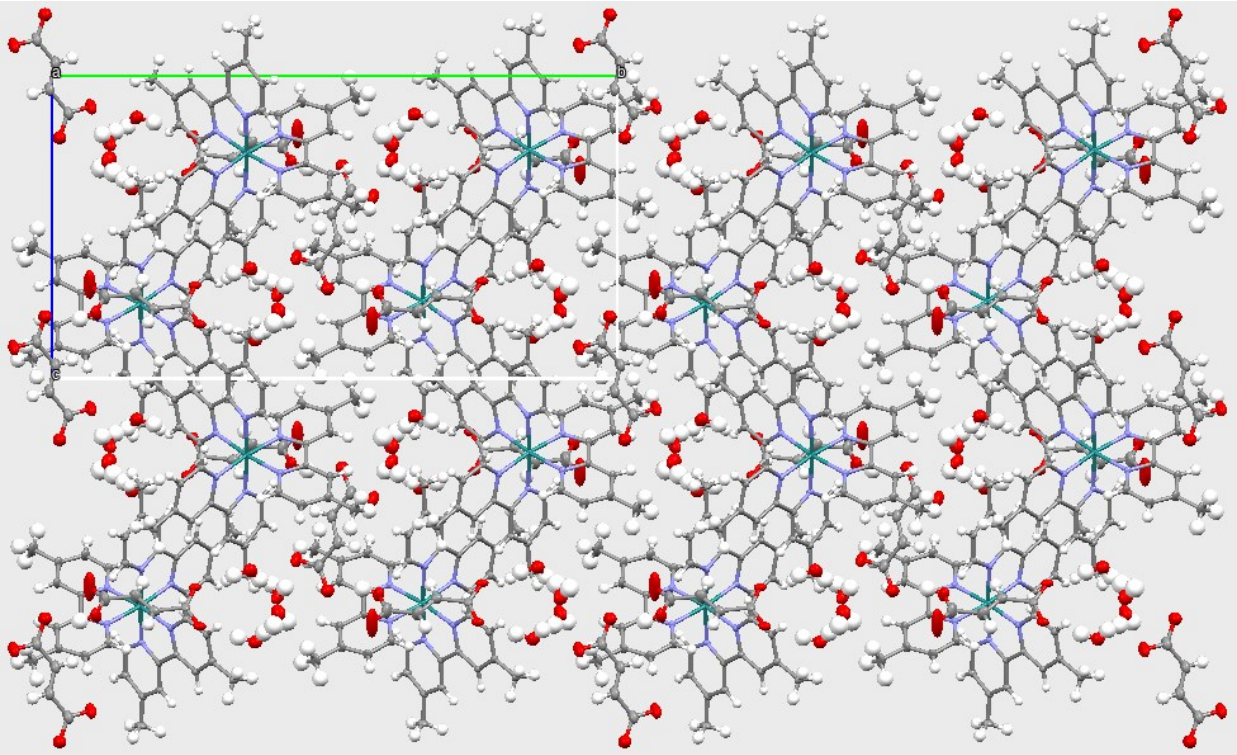

Figure S11 Simulated powder pattern of **2a** with help of the Mercury software[1] based on the single crystal structure of **2a**.

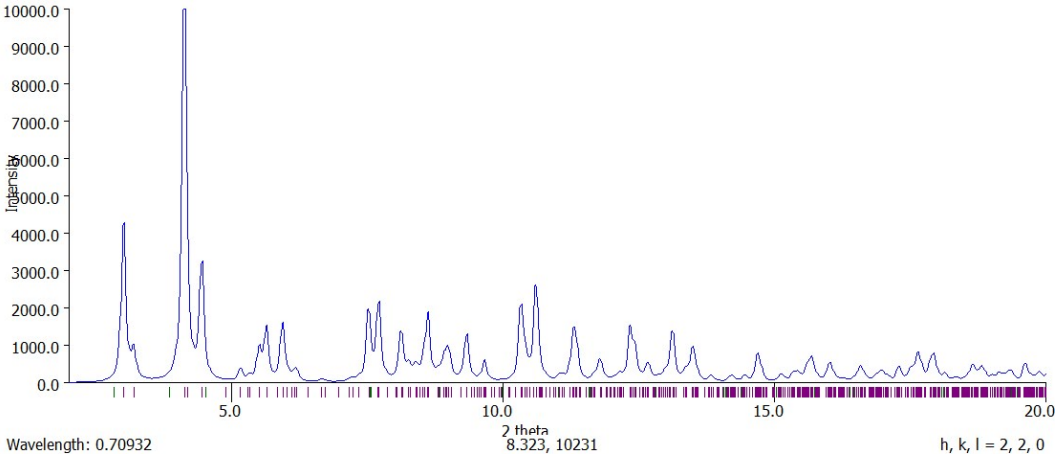

Figure S12 Measured PXRD pattern of **2a** synthesized on a macroscopic scale as described above.

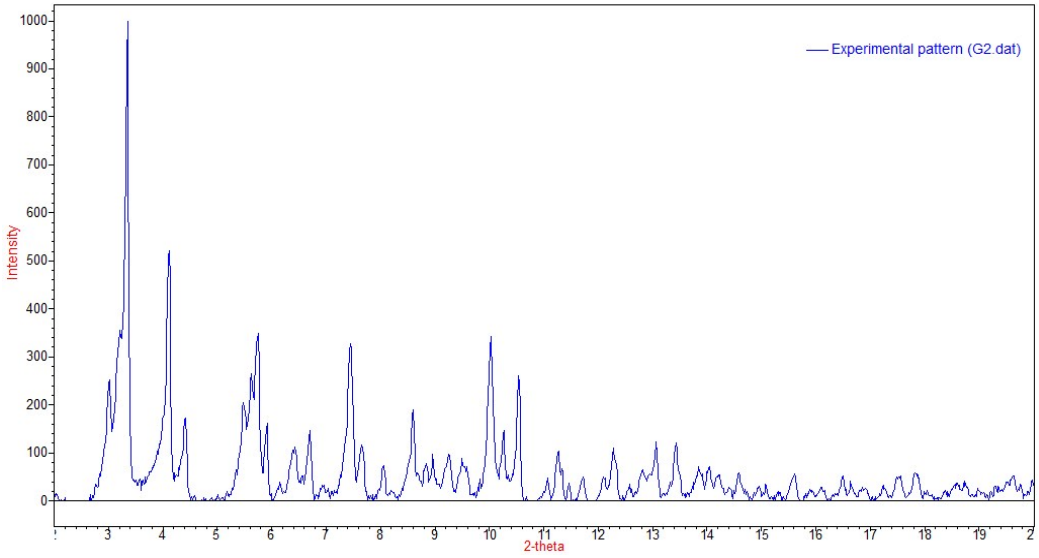

S5 Ruthenium(II) tris(4,4'-dimethyl-2,2'-bipyridine) saccharinate tetrahydrate (2b)

Single crystals of **2b** were obtained from the high throughput screening method for nano-crystallization of salts by vapor diffusion at 20°C of 500 nL of a 90% saturated solution of **2** in water mixed with the same volume of a 1.57 M solution of sodium saccharinate against a reservoir of a 1.57 M solution of sodium saccharinate. The crystallographic data are summarized in Table S2. **2b** crystallized in the triclinic space group $P\bar{1}$. The asymmetric unit consists of one ruthenium(II) tris(4,4'-dimethyl-2,2'-bipyridine) cation, two saccharinate anions and four water molecules.

A macroscopic synthesis of **2b** was done as follows: The column for the ion exchange was packed with Dowex X1 (Fluka) in H_2O. Subsequently, the column was loaded with saccharinate ions (50 mL, saturated aq. solution of saccharin sodium salt). Then, ruthenium(II) tris(4,4'-dimethyl-2,2'-bipyridine) dichloride tetrahydrate (**2**, 101.1 mg, 0.127 mmol) was dissolved in H_2O (20 mL), passed through the column and dried under reduced pressure to yield ruthenium(II) tris(4,4'-dimethyl-2,2'-bipyridine) disaccharinate · 4.5 hydrate (**2b**, 116.4 mg, 0.106 mmol) as red crystals (yield: 84%).

IR (neat): 3050*w*, 2919*w*, 1619*m*, 1579*m*, 1478*w*, 1447*w*, 1329*w*, 1257*m*, 1138*m*, 1116*m*, 946*m*, 832*m*, 760*m*.

EA: calcd. for $C_{50}H_{44}N_8O_6RuS_2(H_2O)_{4.5}$ C: 54.63, H: 4.86, N: 10.19; found: C: 54.57, H: 4.90, N: 10.35.

Figure S13 Packing diagram of **2b**.

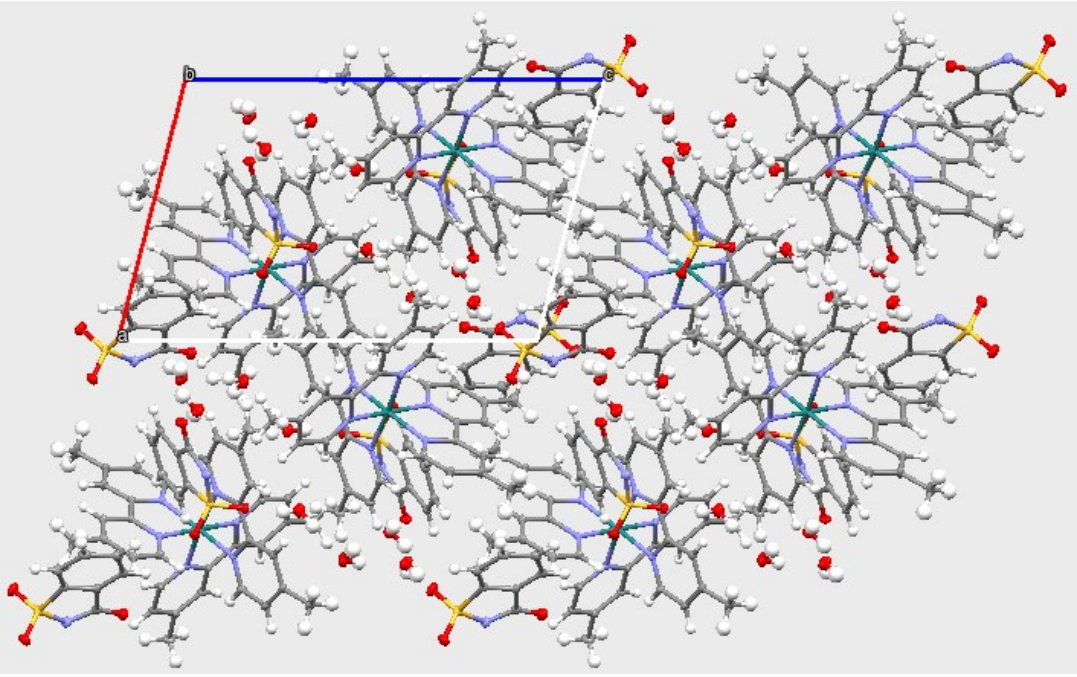

Figure S14 Simulated powder pattern of **2b** with help of the Mercury software[1] based on the single crystal structure of **2b**.

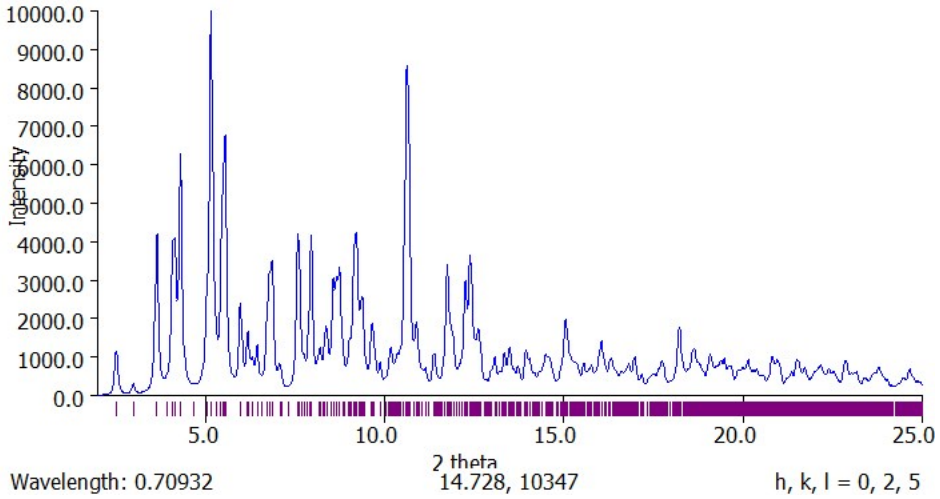

Figure S15 Measured powder XRD pattern of **2b** synthesized on a macroscopic scale as described above.

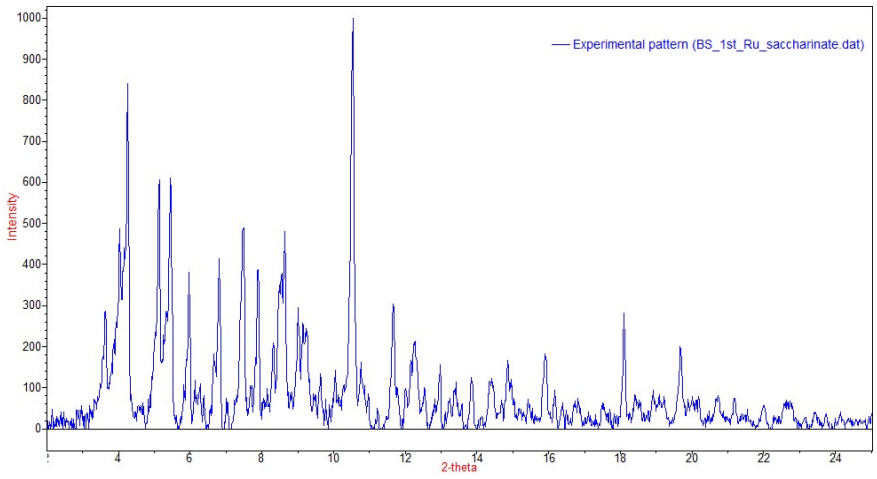

S6 Cobalt(II) bis(2,2'-bipyrid-6'-yl)ketone *p*-toluenesulfonate tetrahydrate (4a)

Single crystals of **4a** were obtained from the high throughput screening method for nano-crystallization of salts by vapor diffusion at 20°C of 500 nL of a 90% saturated solution of **3** in water mixed with the same volume of a 0.15 M solution of sodium *p*-toluenesulfonate against a reservoir of a 0.15 M solution of sodium *p*-toluenesulfonate. The crystallographic data are summarized in Table S3. During crystallization a ligand exchange took place, in which one bromide ligand was replaced by a *p*-toluenesulfonate ligand and the other bromide ligand by an aqua ligand. **4a** crystallized in the monoclinic space group $P2_1/c$. The coordinated water molecule forms hydrogen bonds to one of the co-crystallized water molecules and to an oxygen atom of the coordinated *p*-toluenesulfonate ligand (O34-H34A O35: 2.640(3) Å, O34-H34A O35B: 2.568(8) Å, O34-H34B O33(x,-1+y,z): 2.7180(19) Å).

Figure S14 Packing diagram of **4a**.

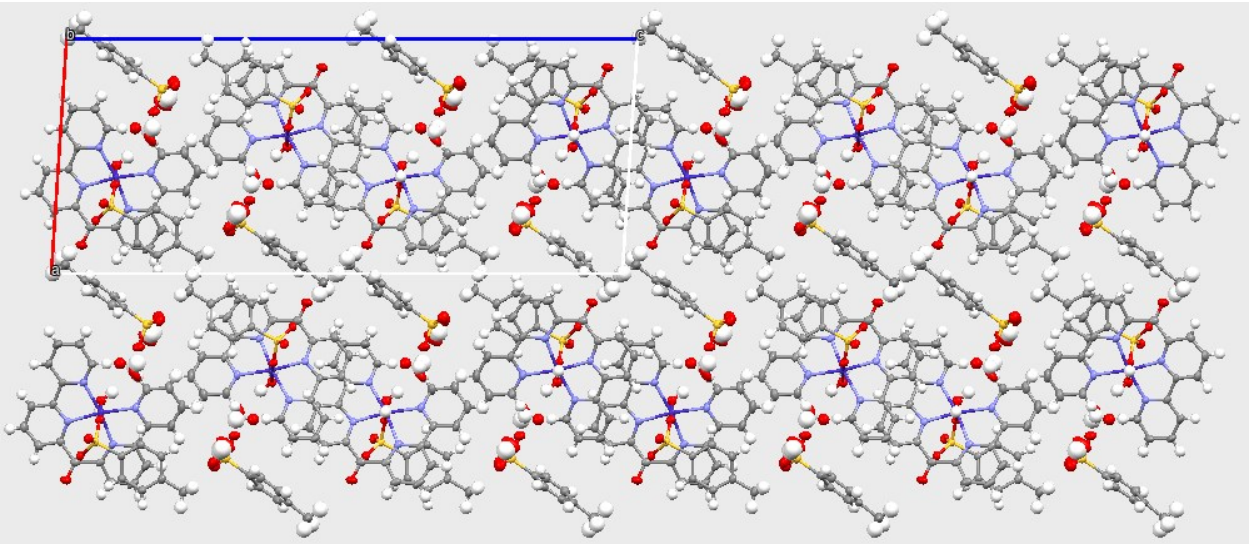

Figure S15 Simulated powder pattern of **4a** with help of the Mercury software[1] based on the single crystal structure of **4a**

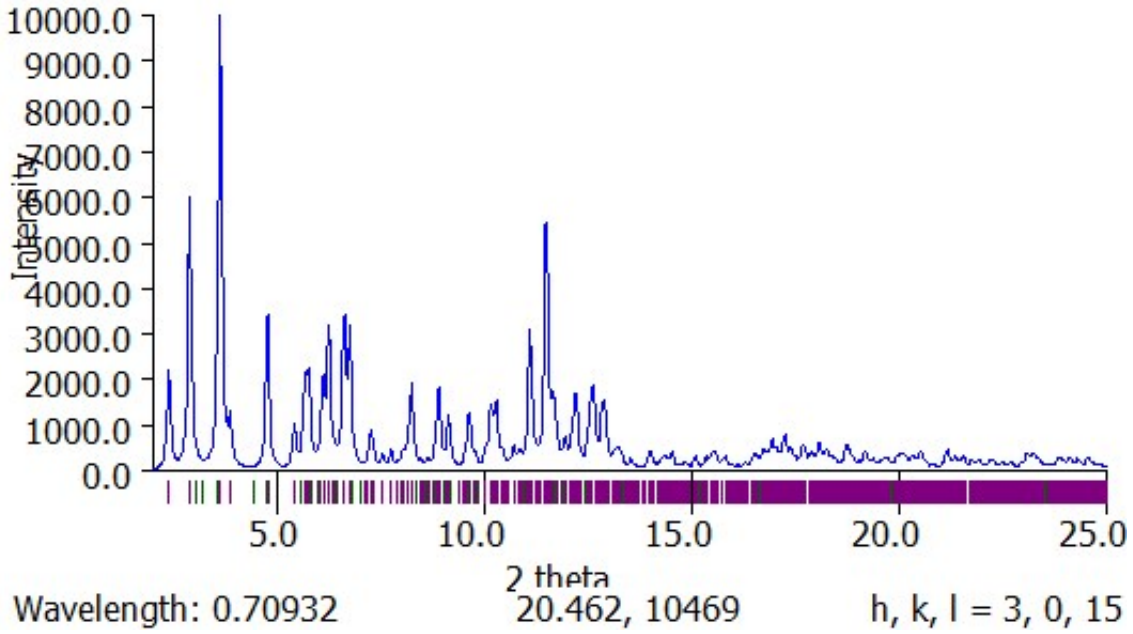

Figure S16 Measured powder XRD pattern of **4a**

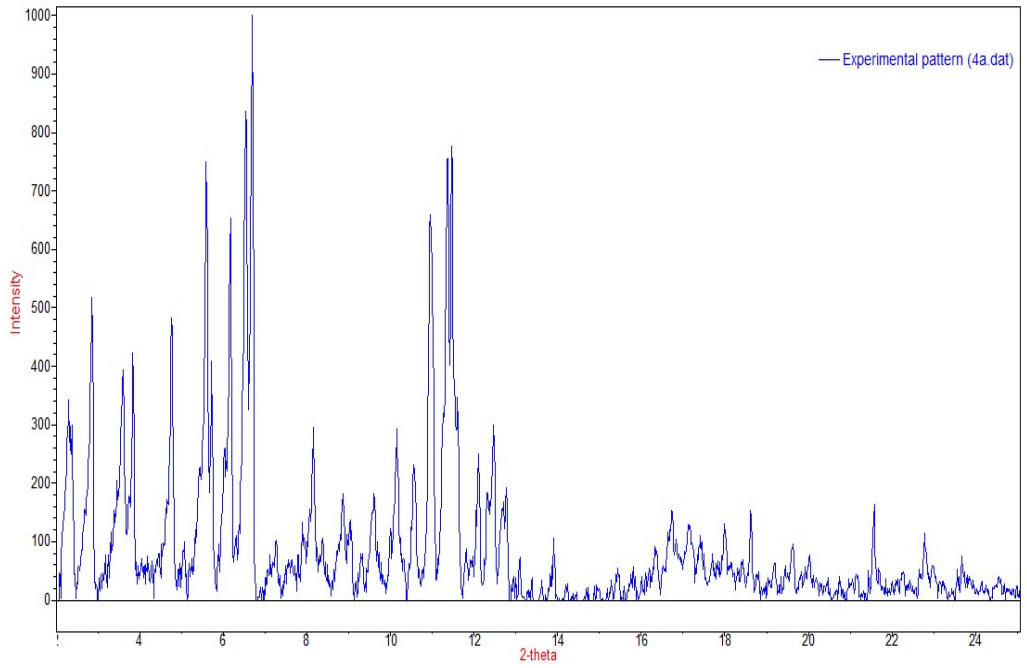

S7 Cobalt(II) bis(2,2'-bipyrid-6'-yl)ketone fumarate · 2.25 hydrate (4b)

Single crystals of **4b** were obtained from the high throughput screening method for nano-crystallization of salts by vapor diffusion at 20°C of 500 nL of a 90% saturated solution of **3** in water mixed with the same volume of a 0.725 M solution of disodium fumarate against a reservoir of a 0.725 M solution of disodium fumarate. The crystallographic data are summarized in Table S3. During crystallization a ligand exchange took place, whereby the two bromide ligands were replaced by a fumarate anion, which bridges two cobalt metal ions forming 1D-chains. This 1D-coordination polymer runs parallel to the a-axis direction. **4b** crystallized in the monoclinic space group $P2_1/c$. The water molecules forms hydrogen bonds to the oxygen atoms of the coordinated fumarate ligand (O35-H35A O33: 2.823(3) Å, O36-H36A O34(x,1.5-y,0.5+z): 2.753(2) Å, O36-H36B O32: 2.779(3) Å).

Figure S17 Packing diagram of **4b**.

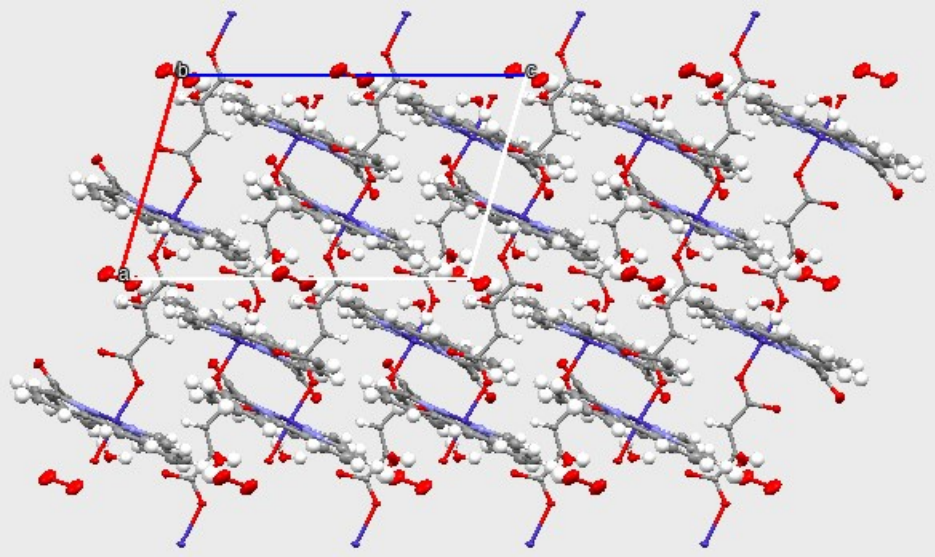

S8 Cobalt(II) bis(2,2'-bipyrid-6'-yl)ketone tetrafluoroborate dihydrate (4c)

Single crystals of **4c** were obtained from the high throughput screening method for nano-crystallization of salts by vapor diffusion at 20°C of 500 nL of a 90% saturated solution of **3** in water mixed with the same volume of a 2 M solution of sodium tetrafluoroborate against a reservoir of a 2 M solution of sodium tetrafluoroborate. As tetrafluoroborate is known to hydrolyze in water[6], it is recommended to use a freshly prepared solution. Additionally, the reaction should be done in plastic vessels, as liberated fluoride might react with glassware to yield SiF_6^{2-}. The crystallographic data are summarized in Table S3. During crystallization, a ligand exchange took place, whereby both bromide ligands were replaced by aqua ligands. **4c** crystallized in the orthorhombic space group *P*bca. The asymmetric unit consists of one cobalt(II) bis(2,2'-bipyrid-6'-yl)ketone cation, two coordinated water molecules and two tetrafluoroborate anions. The coordinated aqua ligands form hydrogen bonds to the fluorine atoms of the co-crystallized tetrafluoroborate anion (O2-H2A F1(0.5+x,y,0.5-z): 2.755(2) Å, O2-H2B F2: 2.697(2) Å, O3-H3A F5B(0.5+x, 1.5-y,1-z): 2.737(4) Å, O3-H3B F7B: 2.669(7) Å, O3-H3B F8: 2.647(8) Å).

Figure S18 Packing diagram of **4c**.

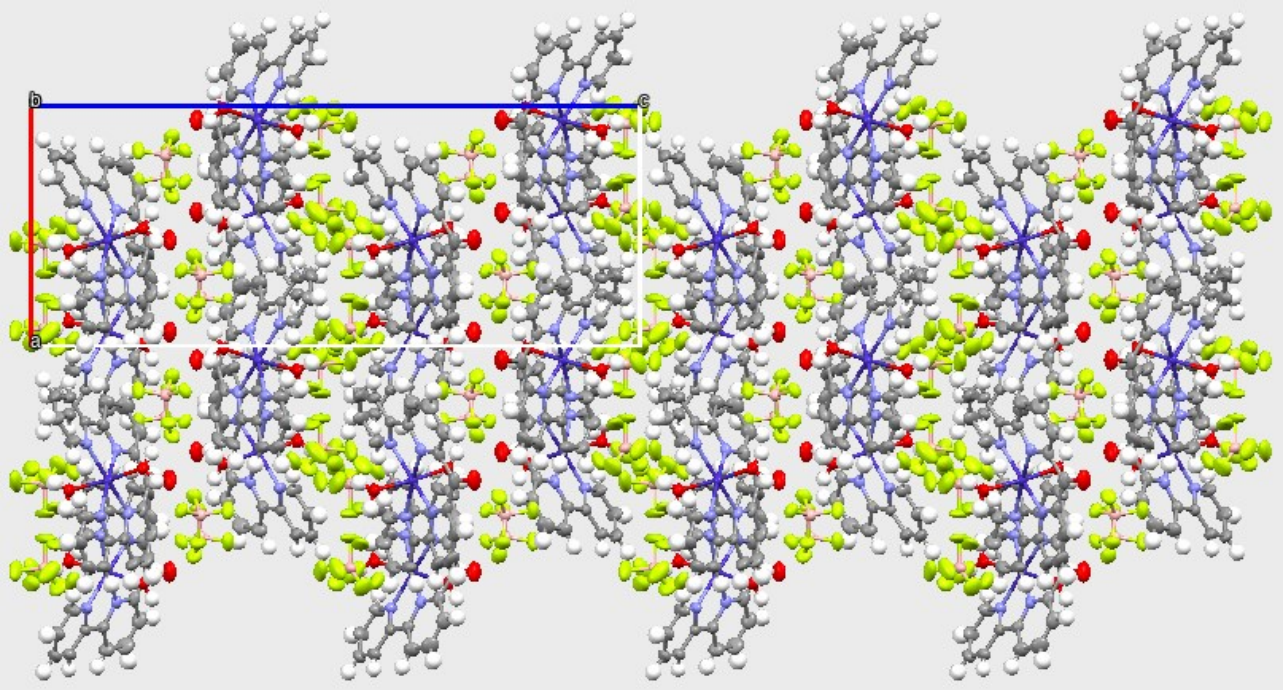

S9 Cobalt(II) bis(2,2'-bipyrid-6'-yl)ketone terephthalate tetrahydrate (4d)

Single crystals of **4d** were obtained from the high throughput screening method for nano-crystallization of salts by vapor diffusion at 20°C of 500 nL of a 90% saturated solution of **3** in water mixed with the same volume of a 0.06 M solution of disodium terephthalate against a reservoir of a 0.06 M solution of disodium terephthalate. The crystallographic data are summarized in Table S3. During crystallization a ligand exchange took place, whereby one bromide ligand was replaced by an aqua ligand and the other bromide ligand by a terephthalate dianion, which bridges two cobalt centers across a center of inversion to form a dimer. **4d** crystallized in the triclinic space group $P\bar{1}$. The asymmetric unit consists of one cobalt(II) bis(2,2'-bipyrid-6'-yl)ketone aqua cation with only half of the coordinated terephthalate, four water molecules and another half of a free terephthalate dianion. The coordinated aqua ligand forms hydrogen bonds to a water molecule and to an oxygen atom of the co-crystallized terephthalate anion and other water molecules. Co-crystallized water molecules form hydrogen bonds to the coordinated terephthalate anion and the oxygen atom of the keto group (O2-H2A O41: 2.7642(15) Å, O2-H2B O31: 2.5825(14) Å, O42-H42B O1(x,y,1+z): 2.9496(15) Å, O43-H43A O34: 2.7719(14) Å).

Figure S19 Packing diagram of **4d**.

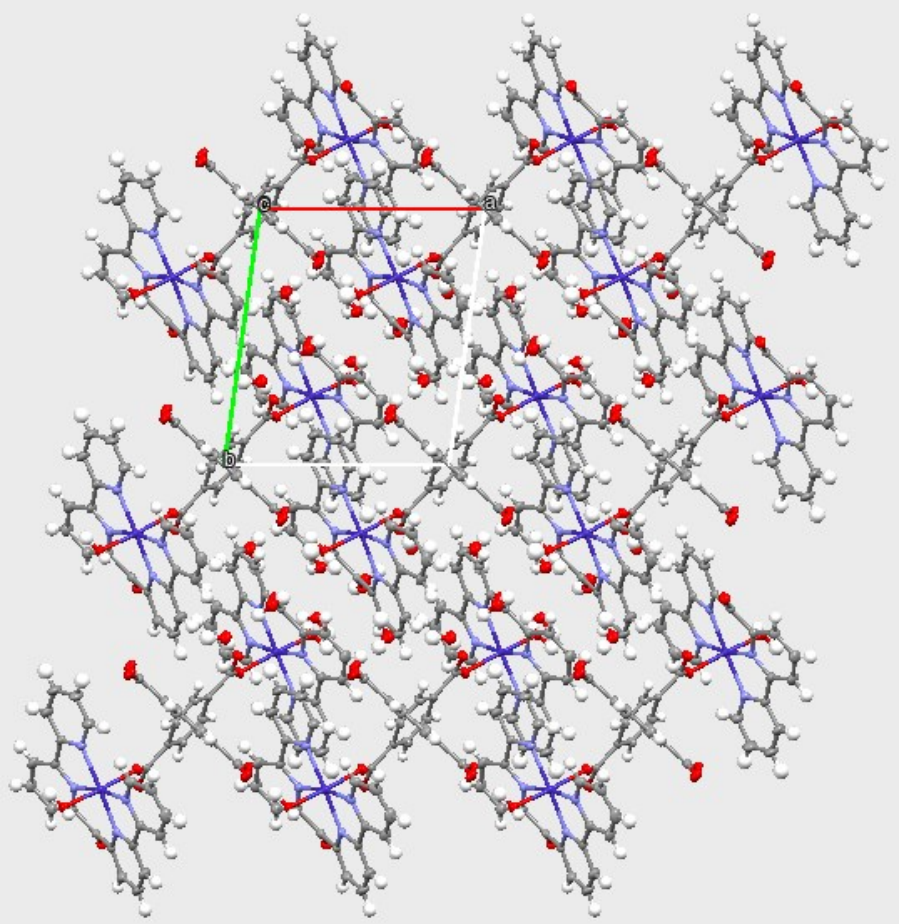

Figure S10 Simulated powder pattern of **4d** with help of the Mercury software[1] based on the single crystal structure of **4d**

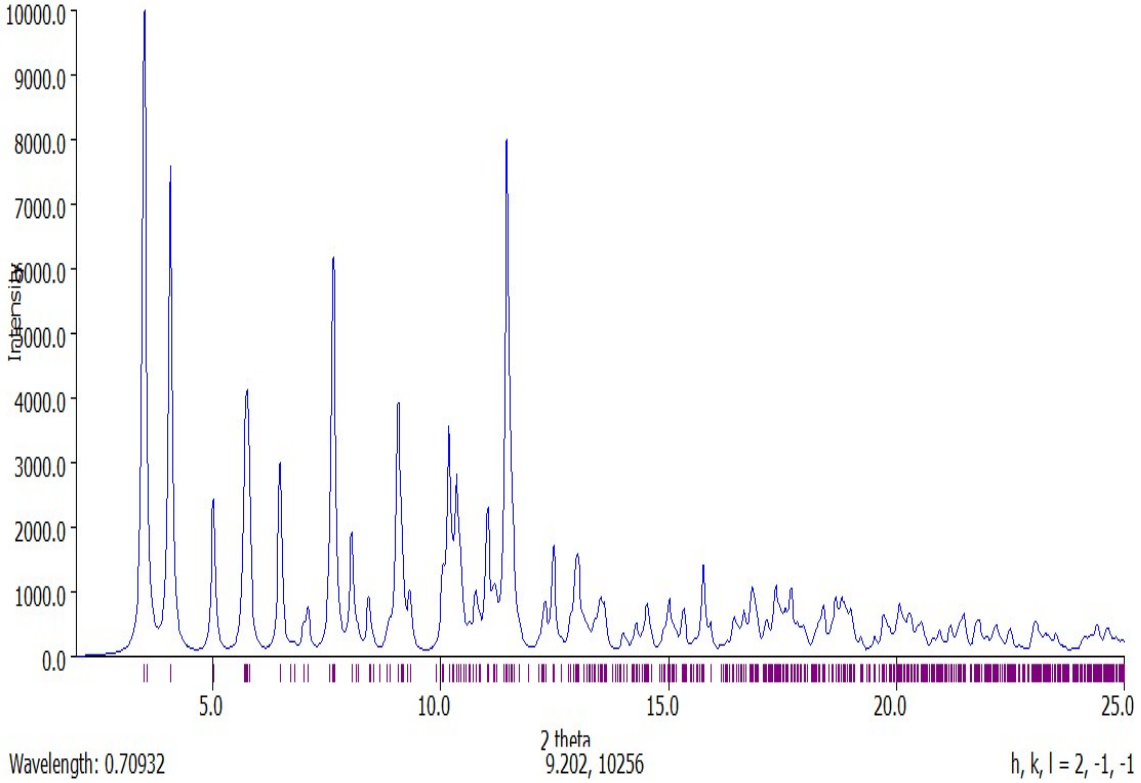

Figure S21 Measured powder XRD pattern of **4d**

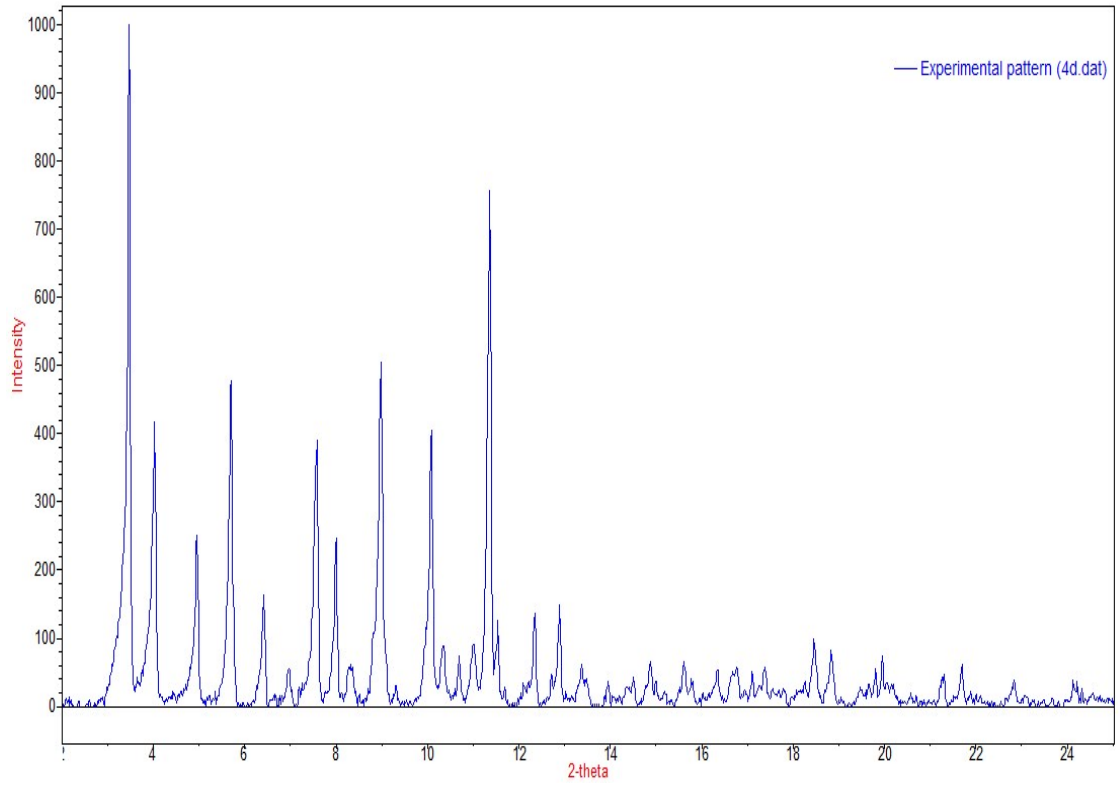

Table S1. Crystal data and structure refinement for **1a**, **1b** and **1c**.

Empirical formula	$C_{32}H_{32}ClCoN_9O_4$	$C_{24}H_{39}CoN_4O_{15}$	$C_{48}H_{73}Cl_{0.5}Co_2N_8Na_{0.5}O_{28.5}$
Formula weight	701.03	682.52	1365.22
Crystal system	Hexagonal	Monoclinic	Triclinic
Space group	P6/mcc	I2/a	P1
a [Å]	13.2910(3)	11.0119(3)	11.0232(3)
b [Å]	13.2910(3)	19.0675(5)	12.5433(3)
c [Å]	21.3987(5)	14.7124(4)	12.8798(2)
α [°]	90	90	96.573(2)
β [°]	90	99.242(3)	109.779(2)
γ [°]	120	90	109.922(2)
Volume [$Å^3$]	3273.66(17)	3049.05(14)	1521.44(7)
Z	4	4	1
Dens. (calc.) [Mg/m^3]	1.422	1.487	1.490
Temperature [K]	160.0(1)	160.0(1)	160.0(1)
Wavelength [Å]	1.54184	0.71073	0.71073
Absorption coefficient [mm^{-1}]	5.292	0.640	0.664
F(000)	1452	1432	713
Crystal size [mm^3]	0.15 x 0.09 x 0.07	0.334 x 0.155 x 0.076	0.214 x 0.139 x 0.096
Crystal description	red block	brownish yellow plate	brownish yellow needle
Theta range for data collection [°]	3.840 to 78.497	2.157 to 33.380	2.147 to 32.031
Index ranges	-16<=h<=14, -16<=k<=16, -26<=l<=26	-16<=h<=16, -28<=k<=27, -21<=l<=22	-16<=h<=16, -18<=k<=18, -19<=l<=19
Refl. collected	1465	35673	87640
Indep. reflections	1465	5416 [R(int) = 0.0454]	20604 [R(int) = 0.0592]
Refl. observed	1358	4592	18139
Complet. to theta	100.0 % to 67.684°	99.9 % to 25.242°	100.0 % to 25.242°
Absorption correction	Semi-empirical from equivalents	Gaussian	Gaussian
Max. and min. transmission	1.00000 and 0.81749	1.000 and 0.532	1.000 and 0.694
Data / restraints /	1465 / 23 / 99	5416 / 6 / 245	20604 / 39 / 885

parameters			
Goodness-of-fit on F^2	1.104	1.049	1.074
Final R indices [I>2 sigma (I)]	R1 = 0.0456, wR2 = 0.1267	R1 = 0.0651, wR2 = 0.1806	R1 = 0.0630, wR2 = 0.1743
R indices (all data)	R1 = 0.0485, wR2 = 0.1294	R1 = 0.0745, wR2 = 0.1864	R1 = 0.0689, wR2 = 0.1784
Absolute structure parameter	n.a.	n.a.	0.015(8)
Largest diff. peak and hole [e.$Å^{-3}$]	0.465 and -0.360	1.354 and -0.708	1.589 and -0.351
CCDC number	1986517	1986518	1986523

Table S2. Crystal data and structure refinement for **2a** and **2b**.

Empirical formula	$C_{84}H_{96}N_{12}O_{20}Ru_2$	$C_{50}H_{52}N_8O_{10}RuS_2$
Formula weight	1795.86	1090.18
Crystal system	Monoclinic	Triclinic
Space group	$P2_1/n$	P-1
a [Å]	10.86902(17)	10.96129(12)
b [Å]	26.9994(3)	14.02802(18)
c [Å]	14.8551(2)	16.6813(2)
α [°]	90	94.3044(10)
β [°]	103.9921(15)	103.1817(10)
γ [°]	90	102.6242(10)
Volume [$Å^3$]	4229.98(11)	2415.90(5)
Z	2	2
Density (calculated) [Mg/m^3]	1.410	1.499
Temperature [K]	160.0(1)	100.00(11)
Wavelength [Å]	0.71073	0.71073
Absorption coefficient [mm^{-1}]	0.435	0.480
F(000)	1864	1128
Crystal size [mm^3]	0.278 x 0.117 x 0.063	0.418 x 0.208 x 0.105
Crystal description	red prism	red plate
Theta range for data collection [°]	2.073 to 35.400	2.530 to 35.486
Index ranges	-17<=h<=14, -43<=k<=43, -22<=l<=24	-16<=h<=17, -21<=k<=22, -26<=l<=26
Reflections collected	113527	63275
Independent reflections	17576 [R(int) = 0.0310]	19867 [R(int) = 0.0245]
Reflections observed	14960	17383
Completeness to theta	99.9 % to 25.242°	99.9 % to 25.242°
Absorption correction	Gaussian	Gaussian
Max. and min. transmission	1.000 and 0.503	1.000 and 0.604
Data / restraints / parameters	17576 / 10 / 551	19867 / 0 / 666
Goodness-of-fit on F^2	1.036	1.035
Final R indices [I>2 sigma (I)]	R1 = 0.0407, wR2 = 0.0996	R1 = 0.0307, wR2 = 0.0736
R indices (all data)	R1 = 0.0495, wR2 = 0.1039	R1 = 0.0380, wR2 = 0.0760
Largest diff. peak and hole [$e.Å^{-3}$]	2.251 and -1.188	0.865 and -0.820
CCDC number	1986525	1986521

Table S3. Crystal data and structure refinement for **4a**, **4b**, **4c** and **4d**.

Empirical formula	$C_{35}H_{34}CoN_4O_{10}S_2$	$C_{25}H_{20}CoN_4O_{7.25}$	$C_{21}H_{18}B_2CoF_8N_4O_3$	$C_{29}H_{28}CoN_4O_{10}$
Formula weight	793.71	551.38	606.94	651.48
Crystal system	Monoclinic	Monoclinic	Orthorhombic	Triclinic
Space group	$P2_1/c$	$P2_1/c$	Pbca	P-1
a [Å]	14.10529(13)	9.89915(12)	11.27579(6)	10.11478(10)
b [Å]	7.34748(6)	14.63676(17)	14.74324(9)	12.22371(13)
c [Å]	34.2057(3)	16.3365(2)	28.71969(18)	12.36967(13)
α [°]	90	90	90	108.5720(9)
β [°]	93.7339(8)	105.9811(13)	90	94.8837(8)
γ [°]	90	90	90	95.9772(8)
Volume [$Å^3$]	3537.50(6)	2275.53(5)	4774.41(5)	1430.47(3)
Z	4	4	8	2
Density (calc.) [Mg/m^3]	1.490	1.609	1.689	1.513
Temperature [K]	160.00(14)	159.99(10)	160.0(1)	160.0(1)
Wavelength [Å]	1.54184	0.71073	1.54184	1.54184
Absorption coefficient [mm^{-1}]	5.455	0.813	6.530	5.279
F(000)	1644	1132	2440	674
Crystal size [mm^3]	0.33 x 0.077 x 0.023	0.242 x 0.168 x 0.143	0.187 x 0.121 x 0.009	0.182 x 0.08 x 0.049
Crystal description	light green plate	red prism	brown plate	brown prism
Theta range for data collection [°]	3.140 to 76.651	2.140 to 35.279	3.077 to 78.831	3.800 to 78.834
Index ranges	-17<=h<=17, -9<=k<=9, -43<=l<=41	-15<=h<=16, -23<=k<=23, -26<=l<=25	-14<=h<=14, -18<=k<=17, -36<=l<=36	-12<=h<=12, -15<=k<=15, -15<=l<=15
Refl. collected	49213	74322	116931	52740
Indep. reflections	7410 [R(int) = 0.0376]	9547 [R(int) = 0.0255]	5136 [R(int) = 0.0470]	5771 [R(int) = 0.0266]
Refl. observed	6718	8924	4604	5667
Complet. to theta	100.0 % to 67.684°	100.0 % to 25.242°	100.0 % to 67.684°	95.2 % to 67.684°
Absorption correction	Gaussian	Gaussian	Sphere	Semi-empirical from equivalents
Max. and min.	1.000 and 0.421	1.000 and 0.682	0.47800 and 0.42466	1.00000 and 0.71041

transmission				
Data / restraints / parameters	7410 / 1 / 498	9547 / 0 / 359	5136 / 0 / 391	5771 / 0 / 428
Goodness-of-fit on F^2	0.999	1.356	1.076	1.080
Final R indices [I>2 sigma (I)]	R1 = 0.0316 wR2 = 0.0766	R1 = 0.0607 wR2 = 0.1281	R1 = 0.0396 wR2 = 0.1088	R1 = 0.0233 wR2 = 0.0650
R indices (all data)	R1 = 0.0365 wR2 = 0.0796	R1 = 0.0637 wR2 = 0.1290	R1 = 0.0441 wR2 = 0.1122	R1 = 0.0238 wR2 = 0.0653
Largest diff. peak and hole [e.$Å^{-3}$]	0.342 and -0.281	0.757 and -0.642	0.568 and -0.374	0.252 and -0.398
CCDC number	1986520	1986519	1986524	1986522

Table S4: Variation of metal-to-metal distances in cobalt(II) bis(2,2'-bipyrid-6'-yl)ketone complexes as a function of the anion, sorted by shortest to longest metal-to-metal distance:

Complex number and axial metal coordination	Cobalt to cobalt distance	Description	Ref.
4d Terephthalate bridged 2 Co, on other side aqua ligand that is bridged by one terephthalate to another aqua ligand	6.8324(3) 8.3070(3) 8.7763(4) 9.2150(3) 10.1148(3) 11.1848(4)	neighbouring columns neighbouring columns neighbouring columns neighbouring columns neighbouring columns bridged by one terephthalate	This work
4a Tosylate on one side, aqua ligand on the other	7.3475(3) 7.8620(9) 8.5396(8) 11.1939(9)	Aqua ligand bonded to tosylate coordinated to Co neighbouring columns neighbouring columns neighbouring columns	This work
4c Aqua ligand bound on each side	7.9998(8) 8.5397(4) 9.0415(7) 10.1413(4) 10.1959(7) 10.2998(6) 11.2758(5)	neighbouring columns neighbouring columns BF_4 bridges two aqua ligands neighbouring columns BF_4 bridges linearly two aqua ligands neighbouring columns neighbouring columns	This work
cobalt(II) bis(2,2'-bipyrid-6'-yl)ketone $(ClO_4)_2$ Aqua ligands on each side	8.0982(9) 8.679(1) 9.170(1) 10.294(1) 11.354(1)		[7]
4b Fumarate anions on each axial side	8.1800(5) 8.1823(4) 9.8168(4) 9.8991(5) 10.3301(5) 10.9326(5) 10.9718(4)	neighbour. columns (U turn of fumarate – H_2O - carboxylate) neighbouring columns neighbouring columns bridged by one fumarate neighbouring columns neighbouring column (bridged by carboxylate - H_2O carboxylate)	This work
cobalt(II) bis(2,2'-bipyrid-6'-yl)ketone $(OTf)_2$ 2 molecules in asym unit. OTf on each side	8.2128(7) 8.2877(7) 8.5950(6) 8.6187(3) 8.9420(7) 9.9498(6) 9.8828(7) 10.6636(6)	 distance between the two metal centres in the a.u.	[8]

	10.7931(7) 11.4584(6) 11.8633(7)		

References

1. C. F. Macrae, L. Sovago, S. J. Cottrell, P. T. A. Galek, P. McCabe, E. Pidcock, M. Platings, G. P. Shields, J. S. Stevens, M. Towler and P. A. Wood, *J. Appl. Cryst.*, 2020, **53**, 226-235.
2. L. Prieto, M. Neuburger, B. Spingler and F. Zelder, *Org. Lett.*, 2016, **18**, 5292-5295.
3. a) P. Kraft, A. Bergamaschi, C. Broennimann, R. Dinapoli, E. F. Eikenberry, B. Henrich, I. Johnson, A. Mozzanica, C. M. Schlepütz, P. R. Willmott and B. Schmitt, *J. Synchrotron Rad.*, 2009, **16**, 368-375; b) C. Brönnimann and P. Trüb, in *Synchrotron Light Sources and Free-Electron Lasers: Accelerator Physics, Instrumentation and Science Applications*, eds. E. J. Jaeschke, S. Khan, J. R. Schneider and J. B. Hastings, Springer International Publishing, Cham, 2016, pp. 995-1027; c) A. Förster, S. Brandstetter and C. Schulze-Briese, *Philos. Trans. R. Soc. A*, 2019, **377**, 20180241.
4. W. Liu, W. Xu, J.-L. Lin and H.-Z. Xie, *Acta Cryst.*, 2008, **E64**, m1586-m1586.
5. A. L. Spek, *Acta Cryst.*, 2015, **C71**, 9-18.
6. M. G. Freire, C. M. S. S. Neves, I. M. Marrucho, J. A. P. Coutinho and A. M. Fernandes, *J. Phys. Chem. A*, 2010, **114**, 3744-3749.
7. J. C. Knight, A. J. Amoroso, P. G. Edwards, R. Prabaharan and N. Singh, *Dalton Trans.*, 2010, **39**, 8925-8936.
8. S. Schnidrig, C. Bachmann, P. Müller, N. Weder, B. Spingler, E. Joliat-Wick, M. Mosberger, J. Windisch, R. Alberto and B. Probst, *ChemSusChem*, 2017, **10**, 4570-4580.